



Publication Year	2016
Acceptance in OA	2020-05-12T08:41:23Z
Title	Cassini's geological and compositional view of Tethys
Authors	Stephan, Katrin, Wagner, Roland, Jaumann, Ralf, Clark, Roger N., Cruikshank, Dale P., Brown, Robert H., Giese, Bernd, Roatsch, Thomas, FILACCHIONE, GIANRICO, Matson, Dennis, Ore, Cristina Dalle, CAPACCIONI, FABRIZIO, Baines, Kevin H., Rodriguez, Sebastien, Krupp, Norbert, Buratti, Bonnie J., Nicholson, Phil D.
Publisher's version (DOI)	10.1016/j.icarus.2016.03.002
Handle	http://hdl.handle.net/20.500.12386/24722
Journal	ICARUS
Volume	274

Cassini's geological and compositional view of Tethys

Katrin Stephan¹, Roland Wagner¹, Ralf Jaumann^{1,2}, Roger N. Clark³, Dale P. Cruikshank⁴,
Robert H. Brown⁵, Bernd Giese¹, Thomas Roatsch¹, Gianrico Filacchione⁶, Dennis Matson⁷,
Cristina Dalle Ore⁴, Fabrizio Capaccione⁶, Kevin H. Baines⁸, Sebastian Rodriguez⁹, Norbert
Krupp¹⁰, Bonnie J. Buratti⁶ and Phil D. Nicholson¹¹

¹ DLR, Institute of Planetary Research, 12489 Berlin, Germany;

² Dept. of Earth Sciences, Inst. of Geosciences, Free University, Berlin, Germany;

³ U.S. Geological Survey, Denver Federal Center, Denver, CO 80225, USA;

⁴ NASA Ames Research Center, Moffett Field, CA 94035, USA;

⁵ Lunar and Planetary Laboratory, University of Arizona, Tucson, AZ 85721, USA;

⁶ INAF-IAPS, 00133 Rome, Italy;

⁷ Jet Propulsion Laboratory, California Institute of Technology, Pasadena, CA 91109, USA;

⁸ Space Science and Engineering Center, University of Wisconsin-Madison, Madison, WI
53706, USA;

⁹ Université Paris-Diderot, 75013 Paris, France;

¹⁰ Max-Planck-Institut für Sonnensystemforschung, 37077 Göttingen;

¹¹ Department of Astronomy, Cornell University, Ithaca, NY 14853, USA;

Running Title: Tethys' geological and spectral properties [<50 characters]

1 **Abstract**

2 [<250 words]

3 The Saturnian satellite Tethys exhibits geological and spectral properties, whose appearance,
4 nature and spatial distribution partly mirror those identified on the neighboring satellites
5 Dione and Rhea or fit to the picture how spectral surface properties are expected to change
6 from one satellite to the other within the inner Saturnian system. However, we also identified
7 spectral variations that are unique in the Saturnian system. Whereas geologically young
8 surface features are characterized by pure H₂O-ice composition with relatively large particles,
9 which match the particle sizes measured for fresh surface features also on Dione and Rhea,
10 geologically old weathered regions are dominated by submicron-sized ice particles. Our
11 investigations confirm that the Odysseus impact event did not cause the formation of Tethys'
12 extended graben system Ithaca Chasma. On the contrary, Odysseus might be responsible for
13 the N-S trending 'icy' bands that mark Tethys' surface in the center of its leading and trailing
14 hemisphere.

15

16 **Keywords**

17 Cassini, VIMS, Tethys, surface composition, geology

18

19

20

1 Introduction

2

3 Since 2004 Cassini has been orbiting the Saturnian system with its instruments detecting the
4 chemical and physical properties of Saturn's atmosphere, its magnetosphere, its satellites and
5 rings. The VIMS instrument especially is the first imaging spectrometer that operates in the
6 Saturnian system, enabling not only the identification of the surface composition but also the
7 mapping of its distribution on the surface of Saturn's satellites. Spectral analyses of Dione,
8 Rhea, Iapetus, Hyperion [Clark *et al.*, 2008; Clark *et al.*, 2012; Cruikshank *et al.*, 2007;
9 Stephan *et al.*, 2010; Stephan *et al.*, 2012] and Enceladus [Jaumann *et al.*, 2008] have made it
10 possible to relate location and extension of spectral units to specific geological and/or
11 geomorphological surface features or characteristics of the space environment – which is
12 essential to resolve the origin of the surface compounds and thus provides valuable
13 information to describe the evolution of the satellite. Although the VIMS spectra of the icy
14 satellites' surface are mostly dominated by H₂O-ice, its distribution and physical
15 characteristics differ distinctly from one satellite to the other [Clark *et al.*, 2008; Clark *et al.*,
16 2012; Jaumann *et al.*, 2008; Stephan *et al.*, 2010; Stephan *et al.*, 2012]. Global hemispherical
17 differences are mostly related to the satellite's position in the Saturnian system, i.e. the
18 distance to Saturn and its E ring, with particles originating from Saturn's magnetosphere
19 and/or the ice grains from the E ring impacting their surfaces [Clark *et al.*, 2008; Stephan *et*
20 *al.*, 2010; Stephan *et al.*, 2012]. Thanks to VIMS mapping capabilities, compositional changes
21 on a regional and local scale can be identified and related to the surface geology. In particular,
22 young or reactivated impact crater and tectonic features – revealing “fresh” (unaltered)
23 surface material - offer a unique view into the crustal properties of its satellite [Stephan *et al.*,
24 2010; Stephan *et al.*, 2012]. Further, the comparison of the physical and chemical surface

1 properties of impact craters emplaced at different times enables to study the alteration of the
2 surface material due to space weathering processes.

3 In this paper we present the analysis of the spectral properties of Tethys in comparison to its
4 geology, which is unique in several ways and completes our investigation of Saturn's inner
5 major satellites. Tethys is 1,062 km in diameter and exhibits a very low density (~ 0.985
6 g/cm^3) [Thomas, 2010] suggesting that the satellite is composed almost entirely of H₂O ice
7 plus a small amount of rock.

8 Tethys is marked by the huge impact basin Odysseus, which is expected to have globally
9 affected surface and internal properties. Odysseus is still discussed as being responsible for
10 the formation of Tethys' prominent tectonic system, Ithaca Chasma [J M Moore and Ahern,
11 1983; J M Moore et al., 2004]. Surface ages, however, indicate that Ithaca Chasma is
12 geologically older than Odysseus [Giese et al., 2007] – speaking against this relationship.
13 Further, the impact crater statistics, at the basis of surface age calculations, are unusual itself.
14 The distribution of small impact craters (1 to 10 km in diameter) is distinctly different from
15 the other Saturnian satellites because the number of these small impact craters is much higher
16 relative to the larger ones [Schmedemann et al., 2014].

17 Finally Tethys has a high albedo value of about 0.8 in the visual spectral range [Verbiscer et
18 al., 2007] indicating a composition largely made of H₂O ice. Possibly, the high reflectivity is
19 enhanced because Tethys collects Saturn's E-ring H₂O-ice particles generated by geysers on
20 Enceladus. Tethys orbits Saturn at a distance of 294,660 kilometers, between the orbits of
21 Enceladus and Dione, and thus is embedded in the E ring environment. Consequently, the
22 comparison of the compositional aspects of all Saturnian satellites provides valuable
23 information for the evolution of the Saturnian system.

24 Key questions about Tethys upon which this investigation is focused to unravel include:

- 1 1. How are Odysseus and Ithaca Chasma spectrally characterized? How are they related to
2 each other? Do the spectral surface properties provide any hint of a common origin and
3 their relation to the history and formation of the body?
- 4 2. Are there any fresh impact craters on Tethys? What are the similarities and differences in
5 the spectral properties of fresh surface features on Tethys compared to fresh impact craters
6 on Dione (Creusa) and Rhea (Inktomi)?
- 7 3. What are the differences in spectral properties between any fresh surface material and the
8 surroundings? What are the resurfacing dynamics and space weathering effects of the
9 satellite?
- 10 4. Are there any hemispherical changes in the spectral properties similar to Dione and Rhea
11 related to the interaction with Saturn's magnetosphere? How do they change from one
12 satellite to the other? What information does it give about the properties of Saturn's
13 magnetosphere?
- 14 5. How do the E ring particles interact with Tethys, which orbits in the middle of it?

15 We start the presentation of our work with an overview of the data set we used (section 2),
16 including the methods used for the spectral and geological analysis. Sections 3 and 4 present
17 the achieved results. In section 3 the identified major geological units are described in detail.
18 In section 4 Tethys spectral properties and the distribution of spectrally different units across
19 Tethys' surface as well as their possible associations to a specific geological – and/or
20 geomorphological features or location on Tethys's surface are discussed. The possible
21 implications for the origin/formation of Tethys's surface compounds and Tethys' evolution
22 are discussed in section 5.

23

1 **2 Cassini data basis**

2 Since 2004, the Cassini spacecraft has been orbiting the Saturnian system exploring Saturn, its
3 magnetosphere and its satellites with numerous flybys at Tethys (Tab. 1). Cassini performed
4 10 (1 targeted and 9 non-targeted) flybys during its nominal mission until 2008, with an
5 altitude between 1500 and about 120,000 km. In particular, Cassini's orbit 47 offered the
6 unique possibility to observe Ithaca Chasma, Tethys' most prominent tectonic features (see
7 below) from a distance of only 16,000 km. Throughout the first extended mission, the Cassini
8 Equinox Mission, from 2009 and 2010, more data were collected during 11 flybys with a
9 closest approach of about 37,000 km during orbit 136, which mainly observed Tethys' trailing
10 hemisphere. In the current second extended mission, the Cassini Solstice Mission, which will
11 continue until 2017, already 7 flybys within distances between about 7600 and 69,000km
12 were successfully performed so far, with orbit 168 offering the possibility to investigate
13 Tethys' largest impact crater Odysseus.

14 **2.1 ISS observations**

15 Spatially highly resolved Clear filter images acquired by the Solid State Imaging Subsystem
16 (ISS) provided not only the geological context but provided the possibility to associate any
17 changes in the spectral properties to specific geographic location, as well as individual
18 geological and/or geomorphological surface features.

19 A digital global mosaic in a simple-cylindrical map-projection of Tethys produced with Clear
20 filter images of the Cassini ISS instrument with a map scale of 0.29 km/pixel, as presented in
21 *Roatsch et al.* [2009], was used as a basis for the global geological mapping procedure as well
22 as the comparison to Tethys' global spectral surface properties. For this purpose we rescaled
23 the mosaic to a lower map scale of 1 km/pixel, which is sufficient for comparison with the
24 global VIMS map since the latter have generally a lower pixel ground resolution than the ISS

1 images. This is the same approach as used for our geologic mapping of Dione and Rhea
2 [Stephan *et al.*, 2010; Stephan *et al.*, 2012]. A map scale of 1 km/pixel is also sufficient to
3 identify global geologic units, individual units within large impact structures (such as basins),
4 and major impact forms. In order to constrain the location of geologic boundaries and in order
5 to characterize a geologic unit as well as to support the investigation of local geological and
6 spectral properties of Tethys, however, we also used the original higher-resolution imaging
7 data to support the mapping procedure. Furthermore, in order to prevent a misinterpretation of
8 VIMS signal due to viewing conditions [Stephan *et al.*, 2012] at the time of the acquisition,
9 simultaneously acquired ISS images were used for comparison.

10 Although not exclusively designed for the development of digital terrain models (DTMs),
11 individual images provide the opportunity to produce DTMs of regional areas using the
12 stereo-technique like the DTM of Ithaca Chasma already presented in the work of *Giese et al.*
13 [2007]. Previous works [Stephan *et al.*, 2014; Stephan *et al.*, 2012] showed the potential in the
14 possibility to associate spectral properties to local topographic changes like slopes, etc.,
15 especially in tectonically formed regions.

16

17 **2.2 VIMS observations**

18 During orbit 15 (September 2005), the only targeted flyby at Tethys, the Cassini spacecraft
19 reached the minimum distance of 1503 km. Most of the non-targeted flybys occurred at a
20 distance between Tethys's surface and the Cassini spacecraft from 57,000 and 52,000 km.
21 These observations cover most of Tethys' surface except the northern polar region (Fig.1).
22 Phase angles of these observations range between 30° and 90° (Fig. 1), which are sufficient
23 for the spectral analysis. Pixel ground resolutions of these VIMS observations do not exceed
24 50 km. They enable at least a global view of Tethys' geological and spectral properties, such

1 as hemispherical differences. Non-targeted flybys, however, which occurred at distances to
2 Tethys closer than 25,000 km, are offering a geological and spectroscopic analysis at least on
3 regional scale. VIMS data for Ithaca Chasma region acquired during Cassini's 47th orbit in
4 June, 2007, cover the canyon system between 60°S and 80°N with ground resolution of about
5 40 km/pixel. These observations also include Telemachus, a relatively large (92 km in
6 diameter) and a morphologically fresh impact crater, which lies at the northern end of the
7 Chasma (54°N/339.4°W).

8 During several non-targeted flybys (Cassini orbits 94, 119, 136 and 164) in the extended
9 "Equinox" mission (2009 - 2010) and in the recent Cassini Solstice Mission (2010-2017)
10 VIMS has acquired data with ground resolution of better than 20 km/pixel, showing us a
11 unique view of Tethys' trailing hemisphere. During orbit 168 (Cassini Solstice Mission)
12 VIMS observations revealed details of Tethys' impact crater Odysseus (32.8°N/128.9°W) on
13 the satellite's leading hemisphere, which, with a diameter of 445 km is the largest impact
14 crater on this body. Unfortunately, being at the terminator, Odysseus was not fully illuminated
15 during the acquisition. As a consequence of this, the western portion of the crater is hidden on
16 the night side.

17

18 [Figure 1 – VIMS coverage + phase angle]

19 [Table 1 – Tethys targeted and non-targeted flybys with VIMS data included in this study]

20

21 ***2.3 Processing and Spectral Analysis of VIMS data***

22

1 VIMS data were radiometrically calibrated, i.e. converted from raw data numbers (*DN*) into
2 physical values of reflectance (*I/F*) by the VIMS team using the latest instrument's spectro-
3 radiometric response function [*Brown et al.*, 2004; *Stephan et al.*, 2010]. In order to attribute
4 variations in the spectral properties to the corresponding geographic locations and to combine
5 the VIMS data set with the Cassini ISS base map [*Roatsch et al.*, 2009] and individual ISS
6 images, each individual VIMS cube is geometrically re-projected, converted into a map-
7 projected VIMS cube following the procedure of *Jaumann et al.* [2006], and finally combined
8 into a global Tethys VIMS mosaic that fits the global ISS base map.

9 Like most of the Saturnian satellites, Tethys' surface is substantially covered by H₂O-ice, the
10 main focus of this study. Its major absorption bands at 1.04, 1.25, 1.5, 2, 3 and 4.5μm
11 dominate every VIMS spectrum. These H₂O-ice absorptions are known to be sensitive to
12 abundance, size and crystallinity of the ice particles, affecting the slope of spectral continuum,
13 the depth and wavelength position of these absorptions. Our goal is to measure the individual
14 spectral parameters of H₂O-ice in the VIMS spectra and map their variations across Tethys'
15 surface on a pixel by pixel basis in order to investigate the observed pattern with respect to
16 possible associations to a specific location and/or geological and morphological surface
17 features, which is essential for resolving the processes responsible for their formation. We
18 concentrate the spectral analysis on specific spectral parameters of the H₂O-ice spectrum,
19 which were already successfully used for the spectral analysis of icy satellites' surfaces [*Clark*
20 *et al.*, 2008; *Jaumann et al.*, 2008; *Stephan et al.*, 2010; *Stephan et al.*, 2012]. Because the
21 absorptions at 3 and 4.5μm are always saturated we focus on the H₂O-ice absorption bands
22 occurring between 1 and 3μm. In order to compare the spectral properties of Tethys to the
23 previous analyses done for Enceladus, Dione, and Rhea we use the same tools for identifying
24 and mapping existing absorption features, i.e. their spectral parameters like wavelength
25 position and depth [*Jaumann et al.*, 2008; *Stephan et al.*, 2010; *Stephan et al.*, 2012], which
26 we briefly summarize in the following.

1 The band depths (*BDs*) of the individual H₂O-ice absorptions were found to be a good
2 indicator for the relative abundance of H₂O-ice. They were measured according to *Clark et al.*
3 [2003]. Although, the depths of these absorptions are also influenced by the size of the H₂O-
4 ice particles, this effect is mostly masked by the varying abundance of H₂O-ice when an
5 additional absorbing compound like the dark material on Dione and Rhea is mixed with the
6 H₂O ice [*Stephan, 2006; Stephan et al., 2009; Stephan et al., 2010; Stephan et al., 2012*].
7 Nevertheless, it is well known that H₂O-ice is completely transparent at 0.5μm without any
8 significant absorption by the H₂O-ice [*Dozier, 1989*]. Therefore, the geometric albedo at
9 0.5μm is a good indicator, how the abundance of H₂O-ice varies across Tethys' surface. We
10 performed a photometric correction of the VIMS channel at 0.5μm using the function
11 algorithm that the Cassini ISS team applied to their Clear/Green-filter images and which
12 shows Tethys as seen at a wavelength of about 0.568μm [*Porco et al., 2004; Roatsch et al.,*
13 2009].

14 A good approximation of changes in the sizes of the ice particles without extensive spectral
15 modeling can be achieved using the band depth ratios (*BDRs*) of the H₂O-ice absorptions
16 [*Stephan, 2006; Stephan et al., 2009*]. Although, the depths of the individual H₂O-ice bands
17 are influenced by the abundance as well as the size of the H₂O-ice particles, only the particle
18 size appears to affect the ratio of the *BDs* of two of the H₂O-ice absorptions. This assumption
19 is valid for all incompletely saturated H₂O-ice absorptions and in case of a non-ice, visually
20 dark contaminant, which is spectrally neutral in the near-infrared wavelength range. Since
21 Tethys exhibits a high geometric albedo in visible light [*Verbiscer et al., 2007*] this
22 hypothesis is valid. Therefore, only small amounts of a dark contaminant are expected on the
23 satellite's surface. Changes in the physical properties of H₂O ice, like the sizes of the
24 individual particles are of special interest, because they are very sensitive to surface ages and
25 weathering affects [*Stephan et al., 2009; Stephan et al., 2012*].

1 In addition fresh H₂O-ice not covered yet by submicron particles show a distinct Fresnel
2 reflection peak at 3.1μm, which also changes its shape depending on the crystallinity of H₂O
3 ice [Gary B. Hansen and McCord, 2004]. The crystallinity of H₂O ice is also expected to
4 influence the wavelength positions of the H₂O-ice absorptions, in particular in case of the
5 absorption at 2μm, shifting the band to longer wavelengths when the H₂O-ice transforms from
6 amorphous to crystalline H₂O ice [Clark et al., 2012].

7 Finally, spectral slopes [Filacchione et al., 2010; Filacchione et al., 2012; Filacchione et al.,
8 2007] like the slope from the visible spectral range into the ultraviolet spectral range (VIS/UV
9 ratio: $I/F_{0.5\mu m}/I/F_{0.35\mu m}$) changes with increasing contribution of dark non-ice material, as
10 identified on Dione and Rhea [Clark et al., 2008; Stephan et al., 2010; Stephan et al., 2012]
11 but has also been shown to visualize regions on the satellite's surface which have endured
12 enhanced space weathering effects, i.e. impacting dust and particles from Saturn's
13 magnetosphere and E Ring [Schenk et al., 2011; Stephan et al., 2012].

14

15 **3 Overview of Tethys' geological units**

16 ***3.1 The pre-Cassini view of the geology of Tethys***

17 Voyager images of Tethys, taken in the flybys in November 1980 (Voyager-1) and August
18 1981 (Voyager-2), revealed a generally densely cratered landscape and two major landmarks:
19 the graben system of Ithaca Chasma and the 400-km large impact structure Odysseus.
20 Voyager-2 returned images with the highest resolution primarily of the Saturn-facing
21 hemisphere [Batson, 1984]. The southern latitudes of the leading and trailing hemispheres as
22 well as the south polar terrain could not be imaged by Voyager at sufficient resolution.
23 Voyager-based geology of Tethys was described by Smith et al. [1981], Smith et al. [1982],
24 and J M Moore and Ahern [1983] and is briefly reviewed here.

1 The densely cratered terrain shows little variation at Voyager resolution and was mapped as a
2 more or less global unit. Most of the cratered terrain is hilly and rugged with a large number
3 of highly degraded craters [*J M Moore and Ahern, 1983; Smith et al., 1982*]. Odysseus is the
4 largest, basin-sized impact feature 445 km across. Voyager frames show a rim consisting
5 mostly of arcuate scarps, partly double, a central peak complex, and radial crater chains
6 reminiscent of secondary craters. Distinct continuous ejecta could not be discerned.

7 Approximately antipodal to Odysseus, a variety of smoother, less densely cratered plains
8 occurs near the large impact structure Penelope. A zone of rugged terrain has been observed
9 antipodal to large impact basins on, e.g., Mercury, created by seismic shaking during basin
10 formation [*J M Moore and Ahern, 1983*]. A type of such rugged terrain antipodal to
11 Odysseus, instead, is not found on Tethys. The smooth plains at this locale were interpreted to
12 have been resurfaced by material forming the smooth plains [*J M Moore and Ahern, 1983*].

13 Troughs, scarps and lineaments of Ithaca Chasma span approximately 270° around the
14 satellite [*Smith et al., 1982*]. This tectonic structure is up to 100 km wide and has been shown
15 to be several kilometers deep, inferred from shadow lengths [*Smith et al., 1981; Smith et al.,*
16 *1982*]. The morphologically most pronounced part of the structure is located at 0° W and
17 trends approximately north-south.

18 Voyager images show two remarkable albedo and color features. The first one described is a
19 longitudinal dark strip centered at 270° W with an approximate North-South trend. This
20 feature is about 15% lower in albedo and redder with a lower violet/orange ratio than the
21 surrounding terrain [*Buratti et al., 1990; Smith et al., 1981*]. The second feature is an elliptical
22 equatorial band in the leading hemisphere which is darker and bluer (higher violet/orange
23 ratio) than the surroundings [*Buratti et al., 1990; Schenk et al., 2011; Stooke, 1989; 2002*]; the
24 feature is depicted but not explicitly described by *Smith et al. [1981]* and *Smith et al. [1982]*
25 in their preliminary albedo and topography maps.

1
2
3
4
5
6
7
8
9
10
11
12
13
14
15
16
17
18
19
20
21
22
23
24

3.2 Description of the mapped geological units

As described in our previous papers [Stephan *et al.*, 2010; Stephan *et al.*, 2012], geologic units are treated as material units rather than terrain types that (a) were formed by a specific process, or (b) were significantly resurfaced by one or even more processes. Surface morphology, therefore, is an important category to subdivide geologic units, in addition to albedo (or color) as the primary category to discriminate geologic units [Wilhelms, 1990]. Based on these criteria, we identified the following sets of units: (1) cratered plains materials and (2) impact-related materials, including craters and basins.

Also following the procedure in Stephan *et al.* [2010] and Stephan *et al.* [2012], craters and basins are classified by their erosional state into at least three units, a technique that has been widely used for geologic maps published by the U. S. Geological Survey [Lucchitta, 1984; Wilhelms, 1990]. This procedure is described below in more detail.

Although crater counts were not explicitly carried out for this work, crater size distributions were measured on Tethys by some of us and have been published elsewhere [Giese *et al.*, 2007; R Wagner *et al.*, 2013a; R Wagner *et al.*, 2013b]. For stratigraphic purposes, we will use and discuss these results in this paper. Absolute cratering model ages for geologic units, when cited here, are derived from two cratering chronologies, (a) a chronology model with a more or less lunar-like time-dependence of the cratering rate [Neukum *et al.*, 2006; Plescia and Boyce, 1985], and (b) a chronology with a constant cratering rate [Zahnle *et al.*, 2003]. For a detailed discussion of these models the reader is deferred to Dones *et al.* [2009]. The final geological map is presented in Figure 2. In the following the mapped geological units will be described in detail.

1 [Figure 2]

2

3 **3.2.1 Cratered plains materials**

4 **a) Densely cratered plains**

5 The most abundant geologic unit on Tethys are *densely cratered plains (dcp)* whose general
6 characteristics could be defined from Voyager images [J M Moore and Ahern, 1983; Smith et
7 al., 1981; Smith et al., 1982]. Here, this unit has been designated as *dcp* and represents a
8 group in a lithostratigraphic sense [Wilhelms, 1990]. A typical locality is seen east of the basin
9 Penelope, in the quadrangles *Ste-9 Penelope* and *Ste-10 Salmoneus* of the Tethys atlas
10 [Roatsch et al., 2009], which is shown in Figure 3. The unit is gently hilly, undulating, in
11 parts rugged, and generally densely cratered. The hilly appearance results from numerous
12 degraded impact features. The largest of the impact craters could already be discerned in
13 Voyager data [J M Moore and Ahern, 1983; Smith et al., 1981; Smith et al., 1982]. Some of
14 these degraded features are members of crater groups, but the high degradation state does not
15 allow us to exactly define the number of craters in these groups.

16 Cassini ISS data covering regions not very well imaged by Voyager complete a global survey
17 of impact basins on the order of 100 km and larger in diameter in unit *dcp*. Remarkably, these
18 large impact features, except Odysseus, are concentrated on the trailing hemisphere in the
19 regions south of the equator. In addition, higher-resolution ISS images show smaller, fresher
20 and therefore younger craters. As has been observed on Enceladus and Dione [R J Wagner et
21 al., 2012], pairs or clusters of craters at all diameters and degradation states are similarly
22 common on Tethys.

1 Fine-scale tectonic features are a characteristic of unit *dcp*, which is revealed only at higher
2 Cassini ISS resolution. In the locale east of the basin Penelope (Fig. 3), subparallel, narrow,
3 comparatively fresh fractures (white arrows) cut an older set of more degraded and wider
4 troughs, but in turn are superimposed by fresher craters up to ~ 10 km in diameter. In other
5 localities of unit *dcp*, these narrow fractures as well as wider troughs resemble chains of
6 circular or elliptical pits instead and probably are of impact rather than tectonic origin. The
7 geologic boundaries of unit *dcp* are clear-cut with respect to all impact crater forms and to
8 tectonically resurfaced units. However, boundaries between unit *dcp* and other cratered plains
9 materials are difficult to define in some parts, as described in the following.

10

11 [Figure 3]

12

13 ***b) Smooth cratered plains***

14 A less rugged, smoother but still densely cratered variety of the cratered plains is located
15 between Ithaca Chasma and the basin Penelope, centered approximately at the trailing
16 hemisphere. This variety was described for the first time by *Smith et al.* [1982] after the
17 Voyager 2 encounter with Saturn and termed *plains terrain* by *J M Moore and Ahern* [1983].
18 *Smith et al.* [1982] report a lower crater frequency compared to the more rugged and hilly
19 densely cratered plains *dcp*. Furthermore, the spatial extent of this unit was not revealed in
20 Voyager images due to incomplete coverage (see, e.g., the geologic sketch map in *J M Moore*
21 *and Ahern* [1983]).

22 In this work, we termed this unit ***smooth cratered plains (scp)***. As with unit *dcp*, the smooth
23 cratered plains *scp* represent a rock-stratigraphic group. Despite the much higher resolution of
24 Cassini ISS images, the boundary between unit *dcp* and *scp* is not sharp but appears to be

1 gradational over a few kilometers or even tens of kilometers, as described by *J M Moore and*
2 *Ahern* [1983]. On lower resolution images, the boundary is easier to locate and can be
3 transferred to a higher-resolution map by the largest craters along its path. An example of a
4 low-resolution ISS NAC frame, obtained in orbit 069TE, is shown in Figure 4a.

5 The gradational boundary between the two units *dcp* and *scp*, and the characteristics of unit
6 *scp*, are shown at higher resolution in Figure 4b. Five large craters several tens of kilometers
7 in diameter are located within *scp*: Phemius, Polyphemus, Icarus, Ajax, and an unnamed
8 crater between Icarus and Polyphemus. The intercrater plains in *scp*, also between smaller
9 craters, are comparably smooth but the transition to the hilly, rugged densely cratered plains
10 *dcp* is clearly gradational and lacks a sharp distinct contact. Penelope, a basin of type b_2 (unit
11 description see section 3.2.3) superimposes the boundary between the two units. We could not
12 identify a scarp between *dcp* and *scp*, as inferred by *J M Moore and Ahern* [1983], but
13 southeast of crater Ajax the boundary between the two units seems to be enhanced by a very
14 subdued rim. The impression of a scarp in some parts could be an artifact resulting from
15 numerous overlapping crater rims in the hilly terrain of unit *dcp* which are little discernable
16 due to the lower-resolution Voyager images.

17 A color asymmetry at the trailing hemisphere, characterized by a high IR/UV ratio, coincides
18 more or less with the smooth cratered plains *scp* but seems to be more extended than this unit.
19 This color feature has been described by *Schenk et al.* [2011]. In Figure 4c, a color ratio of the
20 trailing hemisphere is shown, including the boundary between *dcp* and *scp* with a dotted line.
21 The boundary between high IR/UV albedo and the surrounding terrain with lower IR/UV
22 appears even less distinct than the *dcp/scp* boundary, somehow fading into the lower IR/UV
23 terrain.

24 [Figure 4]

1
2
3
4
5
6
7
8
9
10
11
12
13
14
15
16
17
18
19
20
21
22
23

c) Lightly cratered plains

A specific variety of cratered plains found in only one location was not distinguishable at Voyager resolution. This variety is less densely cratered at medium and small crater sizes compared to units *dcp* or *scp*. We mapped and termed this unit as **lightly cratered plains**, designated *lcp*. Its exact characterization, as well as mapping its spatial extent, is problematical, however.

The type locality south of Odysseus of unit *lcp* is shown in Figure 5. The boundary of this unit with respect to the densely cratered plains (*dcp*) is very sharp and well defined by an abrupt change in crater frequency from *dcp* to *lcp*. The unit is characterized by a rolling, undulating topography with heavily degraded craters several tens of kilometers across. Furthermore, the unit appears depleted in crater frequency at craters smaller than ~ 20 km. The sharp boundary is approximately linear (seen in an equidistant map projection used for the geologic map in Fig. 2) with more or less rectangular changes in direction reminiscent of a segmented fault.

Except in the area south of Odysseus, the boundary of this unit is difficult to identify and to locate. This is due to the fact that the region between Odysseus, Ithaca Chasma and the 100-km large crater Anticleia (whose location is shown in Fig. 6) was imaged at varying viewing conditions, sun elevations and spatial resolutions, as it is documented in the DLR ISS basemap [Roatsch et al., 2009] and in color mosaics [Schenk et al., 2011]. Towards the south pole, imaging at more or less constant viewing conditions and spatial resolutions is also not complete. Therefore, mapping of unit *lcp* between Odysseus, Melanthius in the south, Ithaca Chasma in the east, and Anticleia in the north has to be regarded as preliminary. Additional

1 images at 200 to 300 m/pxl spatial resolution taken at medium sun elevation as well as more
2 stereo coverage is required to exactly map and characterize the spatial abundance of unit *lcp*.
3 The *dcp/lcp* boundary south of Odysseus is in parts marked by a topographic ridge, possibly
4 an outer ring linked to the formation of Odysseus. This is described and shown in more detail
5 in section 3.2.3.

6

7 [Figure 5]

8

9 ***d) Fractured cratered plains***

10

11 The graben system Ithaca Chasma is a major landmark on Tethys and was first seen in the
12 Voyager 1 encounter images [Smith *et al.*, 1981]. The structure is described as a branching
13 trough featuring terraces more than 1000 km long and 50 to 100 km wide [Giese *et al.*, 2007;
14 J M Moore, and Ahern, J. L., 1983]. Ithaca Chasma follows a great circle, predominantly
15 trends NNE-SSW and is approximately centered at the sub-Saturnian hemisphere,
16 transgressing the equator near long. 0° W. Southward, it nearly extends to the south pole.
17 Northward, the troughs are superimposed by the large crater Telemachus. The major part of
18 the Ithaca Chasma structure on the sub-Saturnian hemisphere is shown in the global ISS map
19 of Figure 2. Here, Ithaca Chasma is approximately 100 km wide and branches into two
20 narrower, ~ 50 km wide troughs southward of 10° S lat. [Giese *et al.*, 2007].

21 We identified and mapped two facies of this unit. The first one, ***fractured cratered plains 1***
22 (***fc_{p1}***), is the most common type and consists of a major terraced trough featuring numerous
23 sub-parallel interior minor scarps and troughs. The type locality of *fc_{p1}* south of the large

1 crater Telemachus is depicted in Figure 6. In a digital elevation model (DEM) derived by
2 *Giese et al.* [2007], the bounding troughs are topographically up to 6 km high with respect to
3 the densely cratered plains *dcp* outside Ithaca Chasma which the authors attributed to flexural
4 uplift. The depth of Ithaca Chasma was found to be on the order of 2 – 3 km, based on this
5 DEM.

6 Ithaca Chasma may have been caused by expansion of internal liquid water as it froze into ice
7 after the surface had already frozen. An alternate theory is that the impact that created the
8 Odysseus Crater also generated forces that created Ithaca Chasma, especially since the chasm
9 is on the opposite side of Tethys from the Odysseus Crater. The chasm and surrounding area
10 are heavily cratered, indicating that it was formed long ago.

11 Results from crater counts discussed by *Giese et al.* [2007] infer that Ithaca Chasma is
12 younger than the densely cratered plains but older than the basin Odysseus, rejecting a
13 possible link between its formation and the Odysseus impact as has been suggested by some
14 authors [*J M Moore, and Ahern, J. L.*, 1983]. Higher-resolution images, as those shown in
15 detail in Figure 6, strongly imply the comparably great age of Ithaca Chasma, documented in
16 the majority of craters within Ithaca Chasma superimposing the tectonic structures [*R Wagner*
17 *et al.*, 2013a; *R Wagner et al.*, 2013b]. Furthermore, crater counts performed in these higher-
18 resolution data confirm this stratigraphic finding, as well as previous results by *Giese et al.*
19 [2007] [*R Wagner et al.*, 2013a; *R Wagner et al.*, 2013b] (see section 5).

20 A second facies was mapped as ***fractured cratered plains 2 (fcp₂)*** northeast of Telemachus
21 where the Ithaca Chasma structure approximately trends west-east. In this part, the trough and
22 the scarps are much more degraded and seem to “fade into” tectonically unmodified densely
23 cratered plains *dcp*. The difference in the state of degradation is clearly visible; therefore a
24 separation between the two facies is justified.

1

2 [Figure 6]

3

4 **3.2.2 Crater materials**

5 The three erosional classes of craters c_1 , c_2 , and c_3 roughly represent an overlapping age
6 sequence, meaning that c_1 craters are generally, but not necessarily older than c_2 craters (same
7 for c_2 versus c_3 craters) [Lucchitta, 1984]. No overlap in time exists for c_3 versus c_1 craters,
8 however. In terms of lithostratigraphy, crater materials can be considered as a supergroup,
9 with the individual erosional classes c_1 , c_2 , c_3 representing a rock-stratigraphic group each
10 [Wilhelms, 1990]. The same subdivision for crater materials was used in Stephan *et al.* [2010]
11 and Stephan *et al.* [2012].

12

13 ***a) Heavily degraded crater materials***

14 A great number of craters on Tethys are characterized by a high state of degradation. This
15 type is termed ***heavily degraded crater materials***, designated c_1 . Type examples are shown in
16 Figure 7a. Rims of these craters are mostly degraded. In some craters, only crater ruins with
17 ring arcs are visible (mapped with dotted lines in the global geological map in Fig. 2). No
18 ejecta are visible. Central peaks are generally absent. Numerous smaller craters superimpose
19 the floors of craters of type c_1 . In some parts, groups of heavily degraded craters occur.

20

1 ***b) Partly degraded crater materials***

2 Another rather common type of impact features are ***partly degraded craters materials***,
3 designated c_2 . Type example is crater *Euanthes* (33 km diameter, lat. 7.86° N, long. 238.91°
4 W) north of Penelope (Fig. 7b). Rims in this type are preserved but may show some
5 degradation. Like in type c_1 , central peaks are mostly absent, except in larger craters (e.g,
6 Ajax, see Fig. 7b). Continuous ejecta are generally obliterated by superimposed smaller
7 craters. Larger examples of c_2 -craters, such as *Euanthes*, do have remnants of continuous
8 ejecta, however. As type c_1 , craters of type c_2 also occur in clusters or groups.

10 ***c) Fresh crater materials***

11 A comparably small number of craters, especially at larger diameters (> 10-20 km) are
12 mapped as ***fresh crater materials***, designated c_3 . These craters have pristine rims, well-
13 developed continuous ejecta and generally central peaks. The floors and continuous ejecta
14 display a low frequency of superimposed smaller craters indicating the relative young age of
15 c_3 -craters. Type example is *Telemachus* (92 km diameter, lat. 54° N, long. 339.38° W) shown
16 in Figure 7c. Another type example is crater *Icarius* (54.5 km diameter, lat. 5.89° S, long.
17 305.85° W; Fig. 4b). At the given resolution 1 km/pixel of the geologic map (Fig. 2), these
18 two craters are the only two features included in the map but at smaller diameters more
19 examples of type c_3 are discernible in higher-resolution images.

20 From crater counts carried out on floor and continuous ejecta of *Telemachus*, cratering model
21 ages of 3.6 ± 0.1 Ga (model by *Neukum et al.* [2006]), 0.74 Ga (Case A; uncertainties: 2.3 Ga
22 (high), 0.2 Ga (low)), and 0.12 Ga (Case B; uncertainties: 0.46 Ga (high), 0.03 Ga (low))
23 (model by [*Zahnle et al.*, 2003]) were derived (see section 6).

1 [Figure 7]

2

3 **3.2.3 Basin materials**

4 An *impact basin* is a large impact feature that generally forms early in the history of a planet
5 or satellite by the impact of a massive body [Spudis, 1993]. The boundary diameter separating
6 craters from basins is set approximately at 300 km on the Earth's moon, and such large impact
7 structures are characterized by (a) a complex morphology, (b) extensive ejecta blankets
8 including secondary crater chains and radial sculptures, and (c) may display several
9 concentric rings of ridges, scarps or graben, therefore are designated as *multi-ring basins*
10 [Spudis, 1993].

11 Large impact structures are also abundant on the icy satellites of Saturn but lack a distinct
12 multi-ring morphology. At least two rings, however, may be common, especially in basins on
13 Iapetus on which most of these large impact features were observed to occur [Giese *et al.*,
14 2008; Jaumann *et al.*, 2009]. Unlike the rocky silicate surfaces of the terrestrial planets,
15 complex crater morphologies and ring structures on icy satellites can be distinguished in
16 impact features smaller than ~300 km but larger than ~100 km, especially on the Galilean
17 satellites of Jupiter [Stephan *et al.*, 2013]. Therefore, we set the boundary between craters and
18 basins on icy moons at a threshold of 100 – 150 km to separate basin from crater units. On
19 Tethys, only seven impact structures significantly larger than 100 km are found. Like the
20 crater units, these six features are classified according to their erosional state, and are
21 designated as b_1 , b_2 , b_3 , from older to younger.

22 In general, impact basins, as shown in detailed geologic maps, are characterized by a set of
23 material units. Especially in those cases where several units can be discerned within a basin at
24 the map scale of 1 km/pixel, we follow the convention established for geologic mapping of

1 the moon to consider each set of deposits associated with a specific basin as a named or
2 unnamed group in a rock-stratigraphic sense, with each individual unit in the basin
3 representing a formation, in turn named or unnamed [Spudis, 1993; Wilhelms, 1990].
4 Each basin and its associated units – similarly a major crater – provides a stratigraphic datum
5 to be selected as a time-stratigraphic base for a subdivision of the geologic history of a body
6 into *systems* and *series* [Wilhelms, 1990]. A suggestion for Tethys' time-stratigraphic column
7 and a sequence of geologic events is presented in Figure 2 and discussed in section 5.

8

9 ***a) Heavily degraded impact basin materials***

10 Three of the seven basins on Tethys can be classified as ***heavily degraded basin materials***,
11 designated ***b_I***. These are characterized by remnants of the basin rim, which may be
12 incomplete, and by remnants of central peak structures. These basins are *Demodocus* (125
13 km, lat. 59.37° S, long. 18.21° W), *Dolius* (190 km, lat. 30.15° S, long. 210.33° W), and
14 *Telemus* (320 km, lat. 34.53° S, long. 356.89° W). Telemus und Dolius are shown in Figure
15 8a and b.

16 The rim of Telemus, as well as that of Demodocus, is cut by the tectonic structures of Ithaca
17 Chasma. Dolius still shows a complete but heavily degraded crater rim and an upbowed basin
18 floor with the remnant of a central peak. At low sun, rim and central peak appear enhanced
19 giving the impression Dolius is much fresher. In images with higher sun, however, the high
20 state of degradation of Dolius is clearly visible justifying its classification as a heavily
21 degraded feature.

22

1 ***b) Partly degraded impact basin materials***

2 Impact features classified as ***partly degraded basin materials***, b_2 , have a pronounced but
3 partly degraded rim and a steep inner scarp. No continuous ejecta are discernible. The
4 superimposed crater frequency can be comparably high as in the surrounding cratered plains.
5 Type locality of unit b_2 is basin *Penelope* (207.5 km diameter, lat. 10.8° S, long. 249.2° W),
6 shown in Figure 8c. Bright fresh ice is exposed at the western interior wall. The eastern rim
7 and interior wall appear much more degraded than the western wall. At higher resolution,
8 fractures are seen to transect the basin, and mass wasting features can be distinguished [*R*
9 *Wagner et al.*, 2013a; *R Wagner et al.*, 2013b]. Apart from Penelope, basin *Melanthius* (250
10 km diameter, lat. 58.5° W, long. 192.6° W) is the only other basin of unit type b_2 .

11 Anaglyph images of Penelope (Fig. 9) clearly show a significantly deeper interior compared
12 to the surrounding cratered plains, mostly likely due to little relaxation. The anaglyphs also
13 reveal remnants of an inner ring approximately 50 km in diameter [*R Wagner et al.*, 2013a; *R*
14 *Wagner et al.*, 2013b]. The northern and southeastern arc of this inner ring is best preserved.
15 In both anaglyphs, the location of a landslide at the interior wall is indicated by a long white
16 arrow. Short white arrows mark fractures cutting through the rim. Another tectonic feature,
17 possibly a fault, transects the basin floor but seems to be absent outside Penelope (black
18 arrows in left anaglyph).

19
20 [Figure 8]

21 [Figure 9]

22

1 ***c) Fresh basin material***

2 The youngest basin unit, ***fresh basin material, b₃***, only has one representative on Tethys. This
3 basin, *Odysseus*, 445 km in diameter and located at lat. 32.8 N and long. 128.9 W was
4 discovered in the first Voyager flyby (Smith et al., 1981). In Figure 8d it is shown in
5 comparison with the other basin units. *Odysseus* is 400 kilometers in-diameter, which
6 represents almost two-fifths of Tethys itself. Usually such an impact could have shattered a
7 solid body suggesting that the internal composition of Tethys was still partially molten at the
8 time of the impact event. The crater's rim and central peak have largely collapsed, leaving a
9 shallow crater, and this also suggests a terrain that was elastic enough to change shape. The
10 subdued features of *Odysseus* are in contrast to many steep cliffs elsewhere. This again
11 suggests that the ancient terrain that was still elastic enough to change shape. Even at a map
12 scale of 1 km/pixel, several units associated with this basin can be identified. In detail, these
13 units described below are shown in Figure 10. These units can be considered as rock-
14 stratigraphic formations of the *Odysseus* group.

16 *Basin rim and continuous ejecta*

17 Images of the *Odysseus* basin at spatial resolutions of ~ 500 – 700 m/pixel show a
18 pronounced undulating rim (Fig. 10). The rim is mostly fresh and sharp except in the eastern
19 and southern part of the basin where it appears slightly degraded, as seen in the stereo
20 anaglyph (Fig. 10, top right). Outside the basin rim, no clear-cut continuous ejecta blanket can
21 be discerned (Fig. 10, detail 1 and 2).

23 *Terrace material*

1 Odysseus features a terraced interior (Fig. 10, detail 1 and 2) which was mapped as terrace
2 material (*bot*). The terraces form gentle to steep-scarped lobes extending towards the basin
3 center. The lobes and scarps are located approximately at a fraction of 75% of the basin rim
4 diameter.

5

6 *Floor material*

7 At low sun under which most of the highest-resolution images (500 – 700 m/pxl) have been
8 taken so far from Odysseus, the floor appears rough, rugged or blocky and features narrow
9 arcuate fractures (Fig. 10, detail 1 and 2).

10

11 *Central peak material*

12 Odysseus is characterized by an elevated complex, including a central peak surrounded by a
13 horseshoe-shaped mountain (Fig. 10, top right, and detail 1). The complex was named
14 *Scheria Montes* [Roatsch et al., 2009]. The central peak and the horseshoe-shaped feature
15 were mapped as central peak material, *bocp*. The horseshoe-shaped mountain has a diameter
16 of approximately 100 km.

17

18 *Discontinuous ejecta materials (secondaries)*

19 Towards the northeast, east, and southeast, chains of kilometer-sized craters radiate away
20 from the basin rim (Fig. 10, top right, detail 3). These chains were mapped as discontinuous
21 ejecta materials (secondary craters), *bocs*. The chains are also distinguishable in Voyager
22 images [J M Moore, and Ahern, J. L., 1983]. Cassini images do not reveal any chains or
23 discontinuous ejecta west of Odysseus.

1

2 *Smooth deposits*

3 Cassini images reveal several smooth, patchy areas associated with the radial crater chains.

4 These features were mapped as smooth deposits (*bcsd*). The origin is unknown, but these

5 features could represent patches of impact melt. The boundaries with respect to the densely

6 cratered plains (*dcp*) are in many places not sharp.

7

8 **4 Tethys' spectral properties**

9 Although every VIMS spectrum of Tethys' surface is dominated by H₂O-ice (Fig. 11), both

10 global and regional/local spectral variations could be identified. Spectral variations occur

11 especially with respect to the *BDs* of the H₂O-ice absorptions and how the *BDs* of the

12 individual H₂O-ice absorptions vary to each other. Due to the dominance of H₂O ice the

13 individual absorption bands at 1.04, 1.25, 1.5 and 2 μ m are distinct and relatively deep in

14 every VIMS spectrum of Tethys' surface confirming more or less pure H₂O ice (Fig. 11).

15 Their *BDs* vary only by 3 ± 1.3 , 6 ± 2.3 , 10 ± 4.2 and $4\pm 2.9\%$, respectively, across the entire

16 surface.

17 As mentioned above the geometric albedo at 0.5 μ m shows any existing changes in the

18 abundance of H₂O ice without the influences of particle ice changes. Existing base maps of

19 Tethys show only slight changes in the visible albedo. It reaches up to 0.9, corresponding to

20 almost pure H₂O ice [Buratti and Veverka, 1984]. Photometric measurements of Cassini data

21 showed that the leading hemisphere of Tethys is about 10–15% brighter than the trailing

22 hemisphere [Buratti *et al.*, 1990; Buratti *et al.*, 1998; Emery *et al.*, 2005].

1 Like the *BDs* of the individual absorptions, also the variations in the *BDRs* are small
2 (*BDR*_{2/1.5μm}: 1.4±0.2; *BDR*_{2/1.25μm}: ±; *BDR*_{1.5/1.25μm}:±). The *BDR* combinations
3 including the absorption at 1.04μm could not be measured everywhere because of the strong
4 dominance of the *BD*_{1.04μm} by noise signal. Nevertheless, in comparison to the VIMS results
5 derived in case of Rhea and H₂O-ice models [*G. B. Hansen, 2009*] *BDRs* measured on Tethys
6 indicate changes in the average radius of the H₂O-ice particles between less than 1μm and 10
7 μm (see section 6).

8 Slight changes in the VIS/UV ratio are either correlated to changes in the H₂O-ice particle
9 sizes or the additional existence of additional non-ice compounds. No absorptions of
10 additional surface compounds other than H₂O ice like observed on Dione and Rhea [*Stephan*
11 *et al.*, 2010; *Stephan et al.*, 2012] could be identified.

12

13 [Figure 11]

14

15 **4.1 Distribution of Tethys' spectral classes**

16 Spectral variations occur either in relation to Tethys' geology, i.e. associated with specific
17 geological/geomorphological surface features or geological units, or they mirror
18 global/hemispherical differences. Based on variations in the spectral parameters across
19 Tethys' surface (Fig. 12 – 13), six global and local regions of unique spectral properties can
20 be distinguished, as described in detail below.

21 ***a) Geologically young impact features***

22 The strongest H₂O-ice absorptions are associated with few small morphologically fresh
23 impact craters or crater walls of larger impact craters like Telemachos (Fig. 11 and 12), which

1 is similar to what has been observed on Tethys' neighboring satellites Dione and Rhea
2 [Stephan *et al.*, 2010; Stephan *et al.*, 2012]. On Tethys, however, the frequency of fresh
3 impact craters is quite low, corresponding to Tethys' geologically old surface (see section 3).
4 *BDR* maps do not show any hint of these fresh impact craters (Fig. 13). This is contrary to
5 what is seen on Dione and Rhea, where fresh impact craters also exhibit relatively low *BDRs*
6 associated to relatively large H₂O-ice particles compared to their surroundings [Stephan *et al.*,
7 2010; Stephan *et al.*, 2012]. However, this might still be valid also for fresh impact craters on
8 Tethys. Here these impact craters lie already within larger regions of relative low *BDRs* i.e.
9 large particle sizes (discussed below) making their identification in the *BDR* map difficult.

10

11 [Figure 12]

12 [Figure 13]

13

14 ***b) Odysseus***

15 Although also rich in H₂O ice, the H₂O-ice absorption in the vicinity of the large impact
16 structure of Odysseus are with $55\pm 5.1\%$ and $62\pm 4.2\%$ for the absorption centered at 1.5 and
17 $2\mu\text{m}$, respectively, slightly weaker than measured for the fresh impact craters but still deeper
18 than measured for most parts of the surrounding areas (Fig. 12). Similar measurements fortify
19 Odysseus' relatively old geological age (see section 3). Despite the complex nature of this
20 impact structure (Fig. 10), no significant spectral variations could be measured within
21 Odysseus. Either Odysseus indeed exhibits uniform spectral characteristics, or any existing
22 variations are not detectable due to the much lower pixel ground resolution of the VIMS data
23 compared to the spatially highly resolved ISS images.

1 Although, the *BDR*s of individual VIMS observations sometimes appear to decrease toward the
2 northwestern portion of the impact structure, it cannot be excluded that this effect is due
3 viewing conditions. The coverage of Odysseus by VIMS observations is very limited. And,
4 especially during Cassini's orbit 126, which offers a full coverage and the spatially best
5 resolved VIMS data, this portion of Odysseus was hidden in darkness on the night side.
6 Nevertheless, major parts of the crater are included in and/or exhibits the same *BDR*s like a N/S
7 oriented band on the leading hemisphere running from the northern to the southern polar
8 region of the satellite, which is discussed in detail below. Interestingly, Odysseus shows also
9 similar *BDR* values, i.e. similar H₂O-ice particle sizes not only like the N/S oriented band but
10 also like the fresh impact craters on Tethys (Fig. 13).

11

12 ***c) Ithaca Chasma***

13 No exclusive spectral signature can be associated to Ithaca Chasma contrary to what has been
14 observed in case of the tectonic surface features on the neighboring satellites Dione and Rhea
15 [Stephan *et al.*, 2010; Stephan *et al.*, 2012]. It is difficult to identify Ithaca Chasma in the
16 global VIMS maps (Fig. 12 and 13). Although it is well pronounced in the ISS data (Figure
17 2), it is almost not distinguishable from the neighborhood on a global scale. Ithaca Chasma
18 was best observed by VIMS in Cassini's orbit 47. Figure 14 shows the resulting VIMS maps
19 overlapped onto the DTM produced by Giese *et al.* [2007], which offers the unique possibility
20 to investigate the spectral properties in comparison to the local topography (Fig. 15).

21 Although changes in the spectral properties are apparent in the region with a light deepening
22 of the H₂O-ice absorption at 1.5 μ m and decreasing of the *BDR* of the H₂O-ice absorptions at 2
23 and 1.5 μ m in the vicinity of the Chasma, these characteristics rather spectrally separate the
24 region westwards of Ithaca Chasma (including the Chasma itself) from the region eastwards

1 of the Chasma. Because of the Chasma's location around 0°W it exactly lies in the area of
2 transition from the leading to the trailing hemisphere. Thus, spectral variabilities possibly
3 mirror hemispherical differences, which exist independent of the Chasma, rather than spectral
4 properties caused by geological surface processes (discussed below).

5

6 [Figure 14]

7 [Figure 15]

8

9 ***d) Oval albedo feature***

10 Voyager images already showed an oval shaped surface feature in the equatorial region of
11 Tethys' leading hemisphere characterized by a slightly darker visible albedo (Fig. 2). Also the
12 VIMS observations reveal a slight decrease in the *BDs* associated to the lower visible albedo
13 confirming a contamination of the H₂O ice by a strongly absorbing species (Fig. 12).
14 However, no absorption feature could be identified (possibly due to the spectral dominance of
15 H₂O ice) that is exclusively associated with the visually dark material (Fig. 11).

16 ***e) N-S oriented bands***

17 As already indicated before, VIMS maps of Tethys show two N/S trending bands of a slightly
18 more pronounced H₂O-ice signature in the central portions of Tethys' trailing and leading
19 hemisphere and stretch from the northern to the southern polar region (Fig, 12). Usually,
20 higher *BD* values indicate more H₂O ice, which corresponds to a higher visual albedo. The
21 albedo map, though, does not show any hint of these bands (Fig. 2). An explanation could be
22 that the changes in the *abundance* of H₂O ice are very small and that changes in the *particle*
23 *size* of H₂O becomes more dominant in the VIMS signal. Indeed, in the *BDR* maps these

1 bands are characterized by a lower *BDR* value indicating larger H₂O-ice particles in these
2 regions (Fig. 13). In all *BD* and *BDR* maps Odysseus is included in the N/S band on the
3 leading hemisphere. On the contrary, Penelope, the geologically older impact basin (section
4 3.2.3) is excluded from the N/S band in the *BD* maps. In the *BDR* map this band appears to be
5 rather independent of Penelope. The transition away from the band in eastern direction cuts
6 the impact basin in N/S direction. The small fresh impact crater described above cannot be
7 distinguished from the N/S band anymore in the *BDR* map implying a similar particle size.
8 These bands appear in numerous VIMS observations acquired during several Cassini flybys
9 verifying that these effect is real and not an artefact of unusual observation conditions.

10

11 ***f) Hemispherical differences***

12 Hemispherical differences in the spectral surface properties of Tethys' like the ones known
13 from the neighboring satellites Dione and Rhea [*Stephan et al.*, 2010; *Stephan et al.*, 2012]
14 can be only identified, when regional spectral differences, as described above, are excluded.
15 These underlying hemispherical differences indicate that the major H₂O-ice absorptions are
16 slightly weaker on the trailing hemisphere. Indeed in the areas W and E of the N/S band on
17 Tethys' trailing hemisphere show the weakest H₂O-ice absorptions measured on Tethys'
18 surface demonstrating the lowest amount of H₂O- ice in the regions. This also indicated by a
19 slightly lower visible albedo in these regions (Fig. 12).

20 In contrast both hemispheres show a similar relatively high VIS/UV ratio (Fig. 13). The
21 shapes of these regions, however, are different than the N/S bands of larger H₂O-ice particles.
22 Thus, these two effects are not related to each other and two processes independently working
23 are responsible for these spectral characteristics. The variations in the VIS/UV ratio across

1 Tethys' surface, however, are similar to have been observed by the Cassini ISS camera
2 [*Schenk et al.*, 2011].

3

4 **5 Discussion – Tethys stratigraphy and geological evolution**

5 The geological units identified on Tethys surface, their characteristics, the nature of their
6 contact to neighboring geological units as well as their measured geological age enable us to
7 reconstruct the stratigraphic relationships between the geological units and thus to shed light
8 into the geological evolution of Tethys. The association of the spectral properties to either
9 geological surface features on a local scale or to hemispheres on a global scale offers a unique
10 possibility to investigate the processes responsible for the observed spectral properties and to
11 further our understanding about the geological history as well as the space environment of the
12 satellite.

13 The oldest geologic unit on Tethys are the densely cratered plains (*dcp*) which in this work
14 were not further subdivided at the image scale of 1 km/pxl used for geologic mapping (Figure
15 2). This unit features numerous craters as well as basins $> \sim 150$ km in diameter of all
16 degradation types. Figure 16 shows a cumulative distribution measured in a sample of unit
17 *dcp* east of Ithaca Chasma, compared to other units [*R Wagner et al.*, 2013a; *R Wagner et al.*,
18 2013b]. Of the four geologic units depicted in this diagram, the cumulative frequency of the
19 densely cratered plains *dcp* is highest next to that of unit *fcp*₁, indicating the age of the
20 fractured cratered plains has an age comparable to that of unit *dcp*. Cratering model ages for
21 *dcp* are on the order of > 4 Ga, more or less independent of the cratering chronology used
22 [*Kirchoff and Schenk*, 2010; *Neukum et al.*, 2006; *R Wagner et al.*, 2013a; *R Wagner et al.*,
23 2013b; *Zahnle et al.*, 2003].

24

1 [Figure 16]

2

3 Although spectral properties indicate no unique surface composition of the *dcp*, this
4 geological unit is included in the extended portion of Tethys's surface that show the weakest
5 H₂O-ice signature and very small H₂O-ice particles with radii <1 μ m (Fig. 13). These sub-
6 micron sized particles are characteristic for all geologically old surfaces on Tethys, which
7 have been exposed to weathering processes for billions of years (see below). Similar results
8 could be measured on Dione and Rhea [Stephan *et al.*, 2010; Stephan *et al.*, 2012]. Our results
9 are consistent with the findings of Clark *et al.* [2012], who identified sub-micron sized H₂O-
10 ice particles on Saturn's icy satellites.

11 Impact crater and basin units *c1*, *b1* and *b2* date back to the formation of this oldest geologic
12 unit, based on their high state of degradation as well as their superimposed crater frequencies,
13 especially on units *b1* and *b2*. In terms of large impact structure density, Tethys is
14 characterized by the unique feature that basins are preferentially concentrated on the southern
15 hemisphere, except Odysseus. The number or frequency of large craters and/or basins on the
16 other mid-sized satellites of Saturn is either too limited (e.g., Mimas, Dione) to infer a
17 spatially preferential occurrence, or they are more or less uniformly distributed across the
18 surface (e.g., Rhea, Iapetus) [Giese *et al.*, 2008; Kirchoff and Schenk, 2010; Stephan *et al.*,
19 2010; Stephan *et al.*, 2012]. Due to the fact that basins of type *b1* and *b2* are still distinct
20 despite their high degradation state it is apparent that they were formed preferentially on
21 Tethys' southern hemisphere. A complete degradation of pre-existing basins on the northern
22 hemisphere is unlikely since no significant difference in morphology and/or crater frequency
23 between northern and southern hemisphere is detectable. Furthermore, measured crater
24 frequencies on Tethys do not show an equilibrium distribution or saturation that could have
25 been responsible for erasing age differences [Schmedemann *et al.*, 2014]. Spectrally, these

1 impact craters and basins cannot be distinguished from their surroundings, which supports
2 their great geological age (Fig. 12 and 13).

3 The smooth cratered plains unit *scp*, like *dcp*, is interpreted as an old unit, but has a lower
4 crater frequency according to Smith et al. (1982). In crater counts performed by *Kirchoff and*
5 *Schenk* [2010] on Tethys, no distinction was made between the densely cratered plains *dcp*
6 and the smooth cratered plains *scp* in their measurements. Because of the antipodal location of
7 unit *scp* with respect to the Odysseus basin, *J M Moore, and Ahern, J. L.* [1983] discussed the
8 possibility that the formation of this major impact basin also caused the formation of the
9 smooth plains. However, no pervasive resurfacing affecting the high density of craters in *scp*
10 caused by the Odysseus impact event is detectable. Seismic shaking from the impact event
11 was cited as the most likely cause for the origin of the smooth plains [*J M Moore and Schenk,*
12 2007], resulting in a process of "smoothing" the former rugged and hilly terrain of unit *dcp*.
13 Other processes such as cryovolcanic resurfacing by liquid material inferred as a possible
14 cause for smooth terrain formation [*Schenk and Moore, 2009*] can be ruled out since the
15 boundary between units *dcp* and *scp* is in most parts gradational. A similar high geological
16 age supported by the fact that both units, i.e. the *scp* and *dcp*, do not show any differences
17 with respect to their spectral signature (Figure 12 and 13). Any differences are probably
18 masked and/or eliminated due to uppermost surface regolith as a result of billions of years of
19 impacts and space weathering processes.

20 We interpret the prominent tectonic feature Ithaca Chasma, mapped in two varieties of
21 fractured cratered plains (units *fcp₁* and *fcp₂*) to have formed early in Tethys' geologic history.
22 The state of degradation of the scarps and troughs and the high density of craters mainly of
23 type *c₁* and *c₂* superimposing these tectonic structures in Ithaca Chasma infer a time or time
24 period of origin prior to Odysseus. A formation as a consequence of impact deformation by
25 the Odysseus impact event, as suggested by, e.g., *Smith et al.* [1981], seems less likely

1 according to measured crater size frequency distributions [*R Wagner et al.*, 2013a; *R Wagner*
2 *et al.*, 2013b]. Older, even Voyager-based measurements of the crater distribution support
3 these results [*Giese et al.*, 2007; *Plescia and Boyce*, 1982]. It could be possible that the high
4 density of craters superimposed on scarps and troughs of Ithaca Chasma was caused by
5 extensive secondary cratering from the Odysseus impact event. However, this can be more or
6 less excluded since the superimposed craters in turn show wide varieties of degradation states
7 and therefore were formed over a prolonged period of time rather than by a single event.

8 Apart from a supposed impact-related origin Ithaca Chasma could have formed from two
9 sources of stress: (1) Freeze expansion of H₂O ice [*J M Moore and Ahern*, 1983] or (2) tidal
10 stress due to a high eccentricity [*Chen and Nimmo*, 2008]. *Giese et al.* [2007] performed
11 stereo analysis using Cassini ISS images in order to determine the lithospheric thickness and
12 heat flux in Ithaca Chasma. Their results are compatible with Ithaca Chasma being an old
13 surface feature, supporting an age from crater counts derived with lunar-like cratering
14 chronology models [*Neukum et al.*, 2006; *Plescia and Boyce*, 1982], which is on the order of
15 4.0 Ga [*Giese et al.*, 2007; *R Wagner et al.*, 2013a; *R Wagner et al.*, 2013b]. A younger
16 formation age for Ithaca Chasma from the application of the constant cratering rate model by
17 *Zahnle et al.* [2003], order of ~3 Ga, has been considered unrealistic, based on a plausible
18 thermal history model and heat flux of Tethys [*Giese et al.*, 2007; *Multhaup and Spohn*,
19 2007].

20 On the other hand, an age younger than ~ 4 Ga could be possible if Ithaca Chasma originated
21 from tidal stress associated with a higher eccentricity in a more recent past (more recent than
22 ~ 4 Ga) due to a 3:2 orbital resonance with Dione [*Chen and Nimmo*, 2008]. The present-time
23 eccentricity is close to zero and Tethys therefore is tidally inactive, despite a resonance
24 between Tethys and Mimas and a resonance between Enceladus und Dione respectively.
25 According to *Chen and Nimmo* [2008] it is not certain how the orbit of Tethys evolved into

1 this present-time orbital configuration from a higher-eccentricity paleo-resonance with Dione
2 possibly accounting for the formation of Ithaca Chasma. In a more recent work [*Zhang and*
3 *Nimmo, 2012*] imply that the impact of Odysseus could have broken a 3:2 Tethys-Dione
4 paleo-resonance.

5 In the VIMS data the major tectonic surface features on Dione and Rhea show a distinct H₂O-
6 ice signature and a distinct morphology similar to fresh impact craters on these satellites
7 pointing to a geologically younger age [*Stephan et al., 2010; Stephan et al., 2012*]. The
8 spectral signature of Ithaca Chasma on Tethys (geologic unit *fc*), however, is almost
9 nonexistent anymore and is probably masked by spectral signatures of the surface caused by
10 younger surface (exogenic) processes (discussed below). On the contrary, Odysseus, as stated
11 above, shows a distinctly icier, i.e. fresher H₂O ice signature. Thus, our measurements support
12 the thesis that the formations of Ithaca Chasma took place early in Tethys' history but before
13 the Odysseus impact event happened. Therefore, both events are unrelated to each other,
14 supporting the results of *Giese et al. [2007]*.

15 The interpretation and definition of the stratigraphic position of the geologic unit mapped as
16 lightly cratered plains (*lcp*) is problematical, mostly due to insufficient imaging, as described
17 above. The boundary between this unit and unit *dcp* is linear and very sharp south of
18 Odysseus, inferring a tectonic influence, as shown in Figures 5 and 17. The subdued
19 morphology of most large craters as well as the low density of smaller craters ($\leq 20 - 30$ km
20 in diameter) indicates a resurfacing process of so far unknown origin. The spatial extent of
21 this unit is also unknown due to the reasons cited above. In the images available at present,
22 Ithaca Chasma seems to abut against the eastern boundary of this unit. Northward and
23 southward, the boundaries of *lcp* with respect to other units must still be considered as
24 preliminary. The fact that both the modified cratered plains units *scp* and *lcp* are located in
25 proximity to Ithaca Chasma suggests that these two units, as well as the fractured cratered

1 plains *fc_{p1}/fc_{p2}* of Ithaca Chasma could have a common origin related to endogenous
2 processes. This needs further study, based on improved ISS image coverage that might
3 possibly become available toward the end of the Cassini mission.

4 Odysseus is the youngest of the Tethyan basins and was formed after the cratered plains
5 varieties. However, the resurfacing process in unit *lcp* that erased most of the mid-sized and
6 smaller craters could have taken place after the Odysseus impact event. Measurements of
7 crater frequencies verify that the basin is younger than Ithaca Chasma, based on the
8 observation that the majority of the craters superimposes the tectonic structures within Ithaca
9 Chasma and assuming that they are primary craters and not Odysseus secondaries [*Giese et*
10 *al.*, 2007; *R Wagner et al.*, 2013a; *R Wagner et al.*, 2013b]. Cratering model ages of Odysseus
11 from crater counts are on the order of 3.8 Ga in the model by *Neukum et al.* [2006], versus 2.1
12 Ga (Case A) and 400 Ma (Case B) in the model according to *Zahnle et al.* [2003] [*R Wagner*
13 *et al.*, 2013a; *R Wagner et al.*, 2013b].

14 The close proximity of obvious secondary crater chains (unit *bocs*) to the basin rim (*boc*)
15 pointing radially away and the apparent lack of an extended continuous ejecta blanket
16 suggests a low impact energy, possibly from a large projectile impacting at a comparably low
17 velocity. *Zhang and Nimmo* [2012] discuss in a more recent paper that the Odysseus projectile
18 might have had its origin within the Saturnian system and possibly represented a small
19 Saturnian satellite, impacting at low ~ 500 m/sec, which implies a planetocentric (Saturno-
20 centric) impactor. The origin of the Odysseus unit designated as *bosd* is uncertain. Here it is
21 interpreted as smooth deposits, possibly impact melt. Areas of *bosd* are spatially close to the
22 secondary chains (*bocs*). Their boundaries are mostly indistinct. Higher-resolution images are
23 necessary for studying these features in more detail.

24 Several geologically old impact basins were observed with Odysseus the only one with a
25 significantly icier spectral signature, pointing to a younger geologic age than most parts of the

1 surface including Ithaca Chasma. Usually, surface features formed due to excavation of
2 subsurface material like during an impact event and tectonic activity are assumed to exhibit a
3 similar spectral signature if the space environment (discussed below) is not much different in
4 these locations. Interestingly, the size of the H₂O-ice particles is relatively large and similar to
5 fresh icy material on Tethys and observed on Dione and Rhea (Fig. 18). Thus, Odysseus'
6 spectral characteristics are interpreted to be a remnant of its primordial surface composition.
7 On the contrary, Odysseus shows the same signature than the N/S oriented icy band, which is
8 located together with Odysseus on Tethys leading hemisphere indicating a possibly
9 relationship with respect to their formation. However, the N/S band cannot be associated to
10 any surface feature and rather points to a space weathering effect, which is discussed in detail
11 below.

12 The geologically youngest surface features like impact craters are characterized by clean H₂O
13 ice of relatively large particle sizes with particle radii of about 5µm (Fig. 18) in contrast to
14 their weathered surroundings, i.e. geologically old regions. Interestingly, H₂O-ice particle
15 sizes measured of fresh impact craters on other Saturnian satellites like Inktomi on Rhea are
16 similar (see below). Assuming this material is freshly excavated subsurface material, the fresh
17 H₂O ice of relatively large particles, imply that the crustal material of these satellites are
18 similarly chemically and physically composed. However, this cannot explain the particle sizes
19 of the H₂O ice in the N/S bands, which lies in the vicinity of Odysseus. This aspect is
20 discussed in the next section.

21

22 [Figure 18]

23

1 After the formation of the cratered plains varieties including the large basins and degraded
2 basins, the majority of impact craters were emplaced and continuously degraded by space
3 weathering as well as micrometeorite bombardment. These craters are mostly of types (units)
4 c2 and c3. Individually, larger craters of these types may be dated by counting smaller
5 superimposed craters in higher-resolution ISS images in order to define their relative position
6 in the stratigraphic column. The youngest craters of unit c3 show a strong correlation with
7 H₂O absorption features in Cassini VIMS data as, e.g., the double crater east of basin
8 Penelope, or Telemachus, the largest c3 crater on Tethys. Telemachus was dated by crater
9 counts. Its cratering model age is ~ 3.6 Ga according to the Neukum et al. (2006) model, or ~
10 700 Ma (Case A) and ~ 100 Ma (Case B) according to the Zahnle et al. (2003) model
11 (Wagner et al., 2013a,b).

12 Weathering of the surface material due to impacting micrometeorites, dust and/or H₂O-ice
13 particles from Saturn's magnetosphere and rings are still actively altering the chemical and
14 physical properties of Tethys' surface material. Thus the hemispherical differences, the E-W-
15 as well as N-S-trending albedo and color features in the low latitudes on the leading
16 hemisphere and on the center of the trailing hemisphere may have formed recently, or, more
17 likely, they have been persisting for a long (>> 1 Ga) time and are subject to a constant
18 removal and re-deposition of material.

19 Differences in the strength of the H₂O-ice absorptions between the leading and trailing
20 hemisphere on Tethys are expected to mirror the influence of the space environment on
21 Tethys' surface properties. Subdued *BDs* of the H₂O-ice absorptions at 1.5 and 2μm due to
22 visually dark material on the satellites' trailing hemisphere were also measured on Dione and
23 Rhea [Clark et al., 2008; Stephan et al., 2010; Stephan et al., 2012]. Dust particles in Saturn's
24 magnetosphere are known to impact their trailing hemispheres and to cause sputtering of

1 H₂O-ice particles, which can result in a tenuous exosphere of O₂ like detected at Rhea [*Teolis*
2 *et al.*, 2010], whereas E-ring grain bombardment brightens the leading hemispheres.

3 The subdued albedo and *BDs* of the equatorial E-W trending band on Tethys' leading
4 hemisphere corresponds to the dark bluish band observed in Cassini ISS data interpreted to be
5 formed by irradiation of the surface by incident MeV electrons, which are expected to rotate
6 in a direction opposite to the main plasma flow [*Schenk et al.*, 2011]. Weathered regions on
7 Tethys are dominated by sub-micron sized H₂O-ice particles (Fig. 18), which confirm studies
8 by *Clark et al.* [2012].

9 On the contrary to what to expect for surface areas experiencing an enhanced bombardment,
10 the N-S trending icy bands show unusual large ice particles similar to fresh impact craters (see
11 above). Usually, relatively large ice particles only occur in regions that did not experience
12 significant space weathering (either there are geologically young or are shielded from micro-
13 meteoritic and/or radiation bombardment) [*Clark et al.*, 2008; *Stephan et al.*, 2010; *Stephan et*
14 *al.*, 2012] or occur in regions of higher surface temperature [*Jaumann et al.*, 2008; *Stephan et*
15 *al.*, 2009]. Neither explanation works for the N-S bands on Tethys.

16 Because of the similar spectral signature like Odysseus, a formation of these bands related to
17 the Odysseus impact event cannot be ruled out. Several authors discussed the influence of the
18 Odysseus impact event on Tethys, which might have caused a temporary non-synchronous
19 rotation of Tethys that has now become synchronous again. No evidence of any surface
20 signature related to an at least temporarily non-synchronous rotation like cycloid linear
21 surface features, as observed on the Jovian satellite Europa [*Hurford et al.*, 2007], could be
22 identified so far. *Zhang and Nimmo* [2012] only propose an ancient episode of heating and
23 deformation on Tethys, which has been attributed to its passage through a 3:2 resonance with
24 Dione and possibly was broken by the Odysseus impact event [*Zhang and Nimmo*, 2012].

1 Since these N-S trending bands occur mostly independent of geological features, they are
2 interpreted as a relatively recently formed. Tethys exhibits some thermal anomalies, with
3 higher surface temperatures corresponding to the low-albedo feature close to the equator of
4 Tethys' leading hemisphere [Howett *et al.*, 2012]. No thermal characteristic can be connected
5 to the N-S bands. The location and overall shape of these bands also do not fit the areas
6 expected to endure enhanced impacts of particles from Saturn's magnetosphere as well as
7 from the E ring. However, Tethys orbits Saturn in the densest part of Saturn's E ring as well
8 as in a region of dense plasma of Saturn's magnetosphere, which might also cause the higher
9 porosity of Tethys' surface compared to the other Saturnian satellites derived from UV
10 measurements [Royer and Hendrix, 2014]. Thus, the interaction between the surface material
11 and the space environment might be more complex here and different from that seen on Dione
12 and Rhea [Stephan *et al.*, 2010; Stephan *et al.*, 2012].

13

14 **6 Summary**

15 Tethys' surface shows geological and spectral surface characteristics, whose appearance,
16 nature and spatial distribution mirror those identified on Tethys' neighboring satellites but
17 partly are unique in the Saturnian system. The geological units are in places associated with
18 the spectral variations of relatively large pure H₂O ice particles in particular at fresh impact
19 craters. Geologically old, weathered regions instead are dominated by very small submicron-
20 sized particles.

21 Our geological investigations confirm that Odysseus with its pronounced morphology and
22 ejecta cannot belong to the oldest features. It is clear that the Odysseus impact event globally
23 affected the satellite, the combination of spectral and imaging data does not support the
24 theories that the Odysseus impact event caused the formation of Ithaca Chasma.

1 But it is not certain yet if the Odysseus impact event is connected to the formation N-S
2 trending ‘icy’ bands that are consistent with Odysseus in abundance and particle size of H₂O
3 ice. These bands cannot be correlated to expected pattern due to recent radiation effects and/or
4 variations in surface temperature. Although, it cannot be excluded that the Odysseus impact
5 event led to their existence, further investigations are needed to identify the processes
6 responsible for their formation and their possible relationship to either Odysseus or the
7 interaction of Tethys’ surface material with Saturn’s rings and magnetosphere.

8

9 **7 Table Captions**

10 Table 1: Tethys Tour Event Summary including Targeted (T) and non-Targeted (nT) Cassini
11 Flybys at Tethys.

12 **8 Figure Captions**

13 Figure 1: Coverage of Tethys by VIMS observations depending on: (*a*) pixel ground
14 resolution and (*b*) phase angle.

15 Figure 2: Global base map of Tethys acquired by the Cassini ISS instrument [*Roatsch et al.*,
16 2009] used for the geological mapping and comparison to Tethys’ spectral properties (*top*)
17 and the achieved geological map (*middle*) and stratigraphic relationships of Tethys’
18 geological units (*bottom*). Names of discussed impact structures: Ajax (Aj); Antinous (An);
19 Dolius (Do); Euanthes (Eu); Eurymachus (Ey); Icarius (Ic); Laertes (La); Melanthius (Me);
20 Nestor (Ne); Penelope (Pe); Phemius (Ph); Polyphemus (Po); Poseidon (Ps); Telemachus
21 (Te); Telemus (Tm).

22

1 Figure 3: Type locality of the geologic unit *densely cratered plains* (*dcp*) east and northeast of
2 the basin Penelope (P). The detailed view reveals the dominantly rugged and hilly
3 morphology and topography of this unit. Fractures of two different types are indicated by
4 arrows (white: narrow, fresh fractures; black: wider, more degraded fractures and troughs).
5 Crosscutting suggests that the narrow fractures are younger than the wider forms. Dotted
6 outlines indicate ruins of heavily degraded craters not classified as crater units c_1 . Crater
7 Euanthes (E) is the freshest crater form in the depicted area and was mapped as c_2 . The
8 location of the type locality of the *dcp* is shown in the global ISS map of Tethys (Fig. 2).

9 Figure 4: **(a)** Low resolution image from orbit 069TE, ISS NAC frame N1590391036, oblique
10 view showing the large fresh crater Telemachus (Te) and the approximately north-south
11 trending graben system of Ithaca Chasma (IC) superimposed by Telemachus; the roughly
12 circular boundary between units *dcp* and *scp* is shown as a dotted line. **(b)** Type locality of
13 unit *scp*, smooth cratered plains; detail of a mosaic of ISS NAC images taken in orbit 119TE,
14 observation sequence GEOLOG001, scale 720 m/pxl (orthographic projection at lat. 2° N,
15 long. 247° W); impact features indicated are Penelope (Pe), Phemius (Ph), Polyphemus (Po),
16 Icarus (Ic), Ajax (Aj), and Euanthes (Eu). **(c)** Color ratio of the trailing hemisphere of Tethys,
17 obtained in orbit 119TE, observation sequence LOWPHASE001, at a scale of 1.4 km/pxl.
18 Ratios of Cassini ISS filters IR3/UV3, IR3/GR and UV3/IR3 are set to red/green/blue
19 respectively. The same craters as in (b) included, plus craters Antinous (An, basin-sized) and
20 Irus (Ir). The location of the type locality of the *scp* is shown in the global ISS map of Tethys
21 (Fig. 2).

22 Figure 5: Type locality of unit *lightly cratered plains* (*lcp*) and its boundary with unit *dcp*
23 (thick arrows). Impact features indicated are the type b_2 basin Melanthius (M), Poseidon (P),
24 Eurymachus (E), and the heavily degraded craters Nestor (N) and Laertes (L). A part of the
25 tectonic graben in Ithaca Chasma (IC), unit *fc_{p1}*, is seen at the right. Part of a mosaic

1 constructed from ISS NAC frames from orbit 026TE with an average resolution of 720 m/pxl.
2 The *dcp/lcp* boundary is shown here as a curved line due to the orthographic projection but is
3 more or less linear in cylindrical map projections as used in DLR basemap (Fig. 2). See also
4 Figure 17 for more details.

5 Figure 6: Detailed image of Ithaca Chasma at higher resolution, showing the type locality of
6 unit *fractured cratered plains (fcp1)*. Part of an ISS NAC mosaic from orbit 047TE, ISS
7 observation GEOLOG002, map scale 120 m/pxl. Further explanation is given in text.

8 Figure 7: Crater material units, mapped according to their erosional state (see text for
9 explanation). **(a)** heavily degraded craters materials, unit c1; some craters are ruins whose
10 rims are barely visible (arrows; in Fig. 2 mapped with dotted lines only). **(b)** Partly degraded
11 crater materials, unit c2; type locality near the basin Penelope, largest crater of this type in the
12 area shown is Euanthes. **(c)** Fresh crater materials, unit c3; typical example of this class is
13 crater Telemachus showing a very low superimposed crater frequency implying a young age.

14 Figure 8: Impact basin material units, mapped according to their erosional state (see text for
15 explanation). **(a)** Heavily degraded basin materials, b_1 ; degraded rim of basin *Telemus*,
16 indicated by white arrows; a degraded central peak is marked by a black arrow. **(b)** *Dolius*,
17 type of heavily degraded basin materials, b_1 , has a full rim preserved and a degraded central
18 peak. **(c)** Partly degraded basin materials, b_2 ; type locality is *Penelope*. **(d)** Type locality of
19 *fresh basin materials*, $b_3 (= bo)$. The only feature representing this type is *Odyseus* and its
20 associated units.

21 Figure 9: Anaglyph images of basin Penelope (type locality of unit b_2). Height exaggeration is
22 higher in the version on the right. The anaglyphs were put together from images obtained in
23 orbit 136TE. For the explanation for marked features see text. To view the anaglyphs, use red-
24 blue glasses (red on left eye, blue on right).

1 Figure 10: Geologic units mapped in Odysseus, the only representative of basin type b_3 . **Top**
2 **left:** Overview of Odysseus, rectangles indicate the location of the details shown in (1) – (3).
3 Mosaic of NAC images from orbit 049TE (570 m/pxl scale). **Top right:** Stereo anaglyph of
4 Odysseus, (orbit 049TE images). **(1)** Detail with units *boc* (rim and continuous ejecta), *bot*
5 (terraces), *bof* (floor), and a radial crater chain, possibly of secondary origin (*bocs*). **(2)** Part of
6 the basin interior with units *bocp* (central peak complex), *bof* (floor material), *bot* (terraces),
7 and *boc* (rim and continuous ejecta). **(3)** Area to the southeast of Odysseus with radial crater
8 chains (*bocs*) and smooth deposits (*bosd*).

9 Figure 11: Average VIMS spectra of spectrally different regions, which can be distinguished
10 in the global VIMS maps of Figure 12 and 13.

11 Figure 12: Global VIMS maps showing the variations in the band depth (*BD*) of the H₂O-ice
12 absorptions centered at (top) 1.25 and (bottom) 1.5 μ m across Tethys' surface.

13 Figure 13: Global VIMS maps showing the variations in the (top) band depth ratio (*BDR*) of
14 the H₂O-ice absorptions at 2 and 1.5 μ m and the (bottom) VIS/UV slope.

15 Figure 14: Close-up view onto Ithaca Chasma – combination of VIMS data with ISS images
16 and DTM.

17 Figure 15: Topographic profiles of the Ithaca Chasma region combined with VIMS results,

18 Figure 16: Cumulative crater size frequency diagram showing the stratigraphic sequence from
19 old densely cratered plains (unit *dcp*), fractured cratered plains in Ithaca Chasma (unit *fcp1*),
20 several units in basin Odysseus (sum of counted areas in units *boc*, *bof* and *bot*, labels as *ody*
21 in the diagram), to the young crater Telemachus (unit *c₃*, sum of areas of measurements on
22 floor and continuous ejecta, labeled as *tlm* in diagram).

1 Figure 17: Geology of the surrounding of Odysseus. **Left:** ISS Nac frame N1481443192 (orbit
2 00BTE, scale 12.5 km/pxl), arrows indicate the second approximately concentric outer ring
3 (ridge) of Odysseus. **Middle:** Mosaic of images from sequence
4 049TE_MORPHO007_PRIME (orthographic projection, center lat. 2° S, long. 120° W, map
5 scale 570 m/pxl; highpass filtered). **Right:** Mosaic of images from sequence
6 026TE_TETHYS002_VIMS (orthographic projection, center lat. 40° S, long. 80° W, map
7 scale 720 m/pxl; highpass filtered). Geologic boundary between units *dcp* and *lcp* indicated,
8 question mark were uncertain (see text). Large craters/basins: Odysseus (Od) and Melanthius
9 (Me).

10 Figure 18: Comparison of H₂O particle sizes of various terrains on Tethys, Dione and Rhea
11 using the H₂O-ice models of *G. B. Hansen* [2009].

12

13

14

15

16

17

18

19

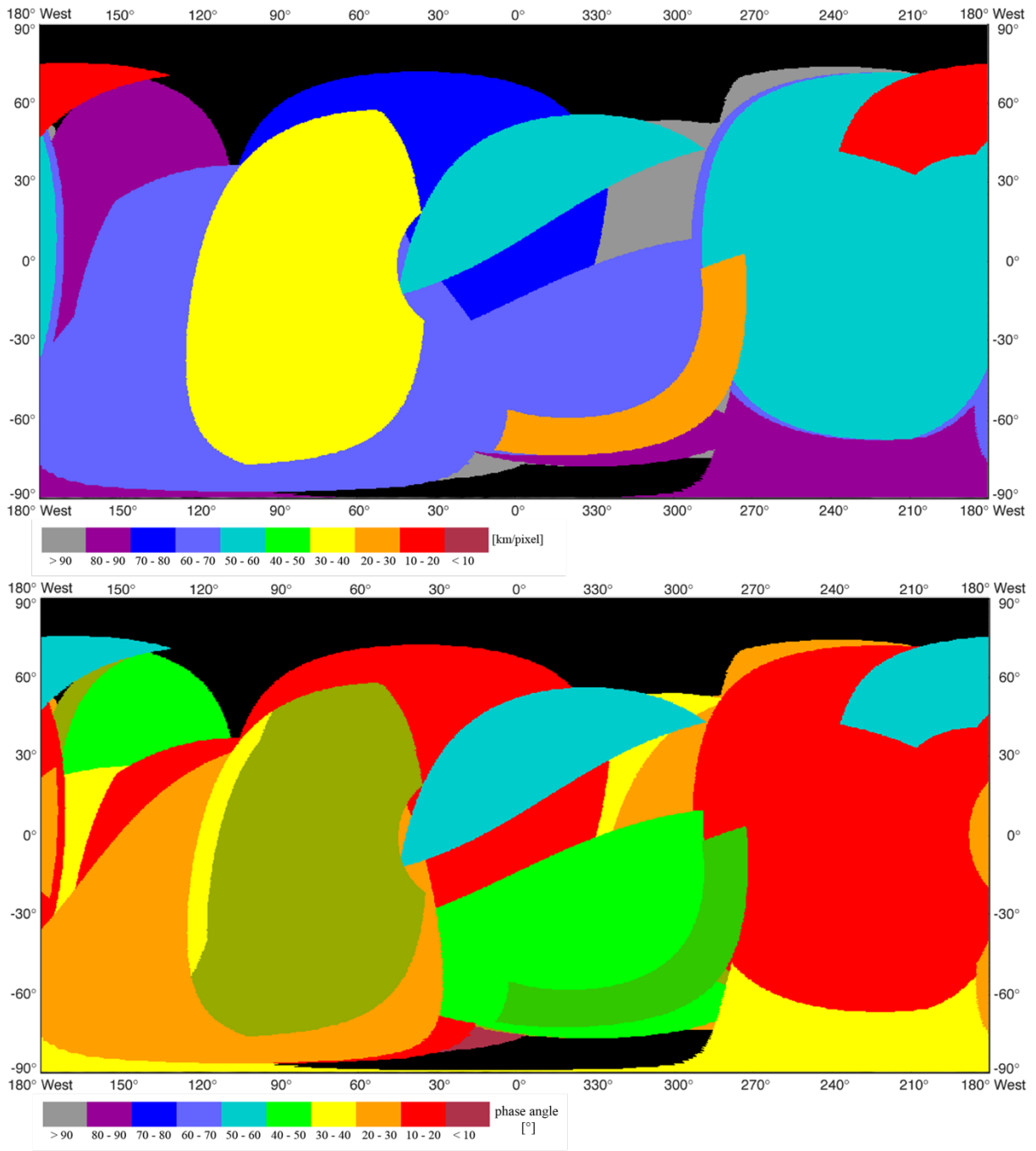
20

1 9 Tables

Mission	Date	Cassini Flyby	Closest	Phase Angle [°]
Nominal	2005-03-09	4 (nT)	83,000	64
	2005-03-29	5 (nT)	109,000	124
	2005-05-02	7 (nT)	52,000	110
	2005-08-20	13 (nT)	123,000	123
	2005-09-23	15 (T)	1500	68
	2006-07-23	26 (nT)	120,000	29
	2007-05-26	45 (nT)	102,000	78
	2007-06-27	47 (nT)	16,000	116
	2007-07-20	48 (nT)	100,000	94
	2007-08-29	49 (nT)	53,000	102
Equinox	2008-09-25	86 (nT)	110,414	50
	2008-10-02	87 (nT)	78,632	70
	2008-11-16	93 (nT)	57,060.9	41
	2008-11-24	94 (nT)	24,233.0	159
	2009-07-26	115 (nT)	68,369.0	89
	2009-10-14	119 (nT)	85,262.7	76
	2009-12-26	123 (nT)	52,923.9	77
	2010-02-13	126 (nT)	111,962.0	114
	2010-04-07	129 (nT)	70,783.7	103
	2010-06-03	132 (nT)	52,611.7	99
Solstice	2010-08-14	136 (nT)	36,965.5	90
	2011-02-20	145 (nT)	45,142.5	123
	2011-08-01	151 (nT)	60,199.9	116
	2011-09-13	153 (nT)	32,606.1	53
	2011-12-12	158 (nT)	60,357.3	140
	2012-04-14	164 (nT)	7,632.4	123
	2012-05-20	166 (nT)	47,701.0	63
	2012-06-28	168 (nT)	68,828.2	79
2015-04-11	214 (nT)	52,863	32	

2 Table 1

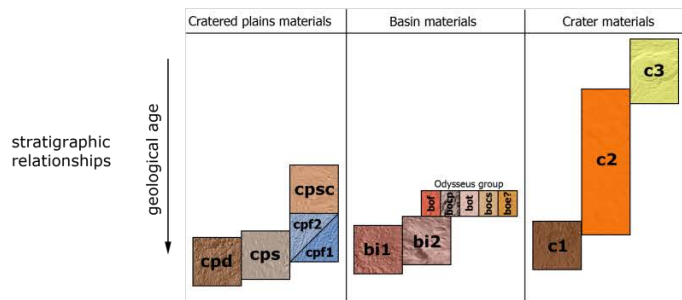
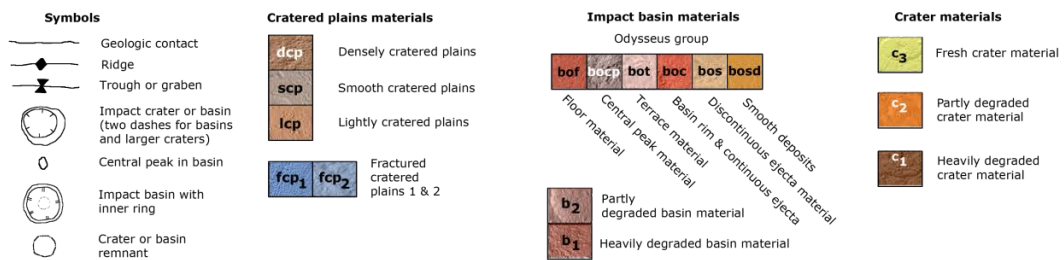
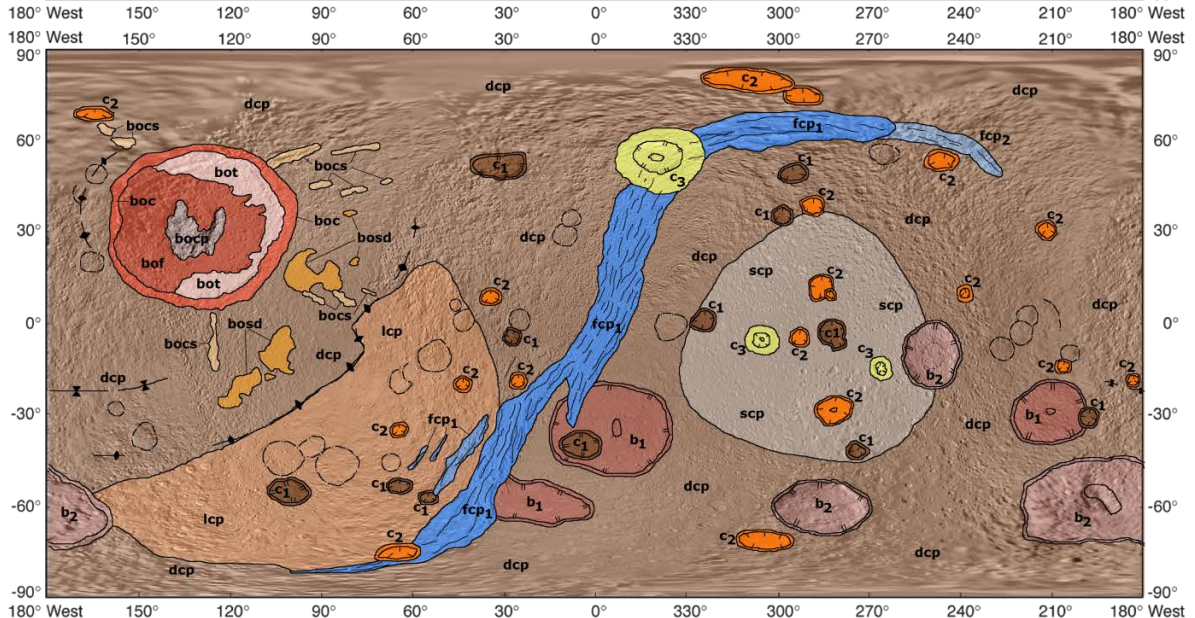
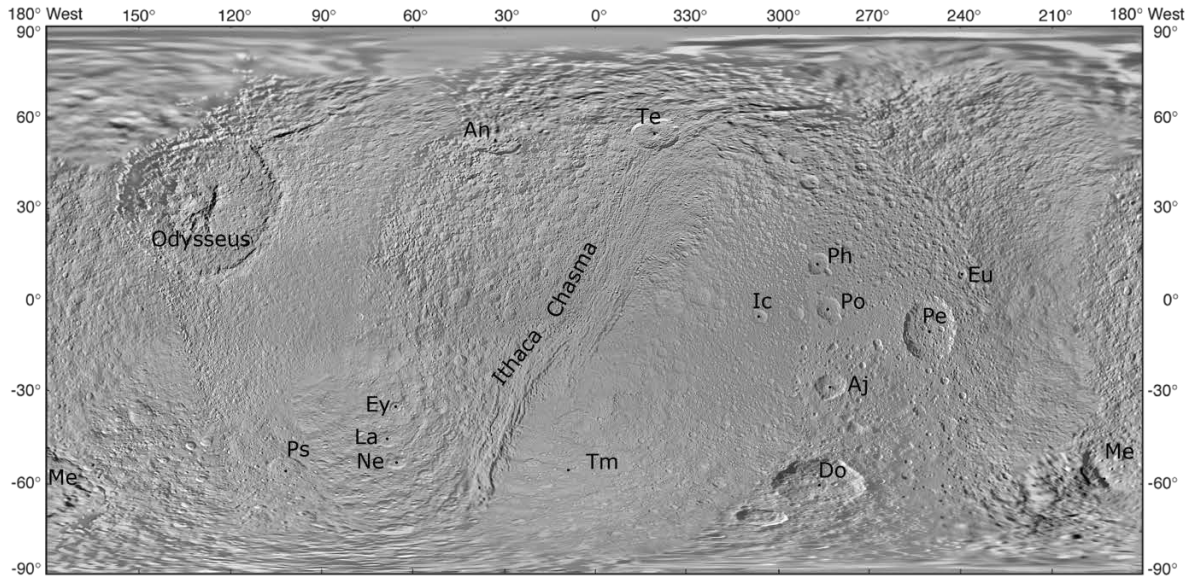
1 10 Figures



2

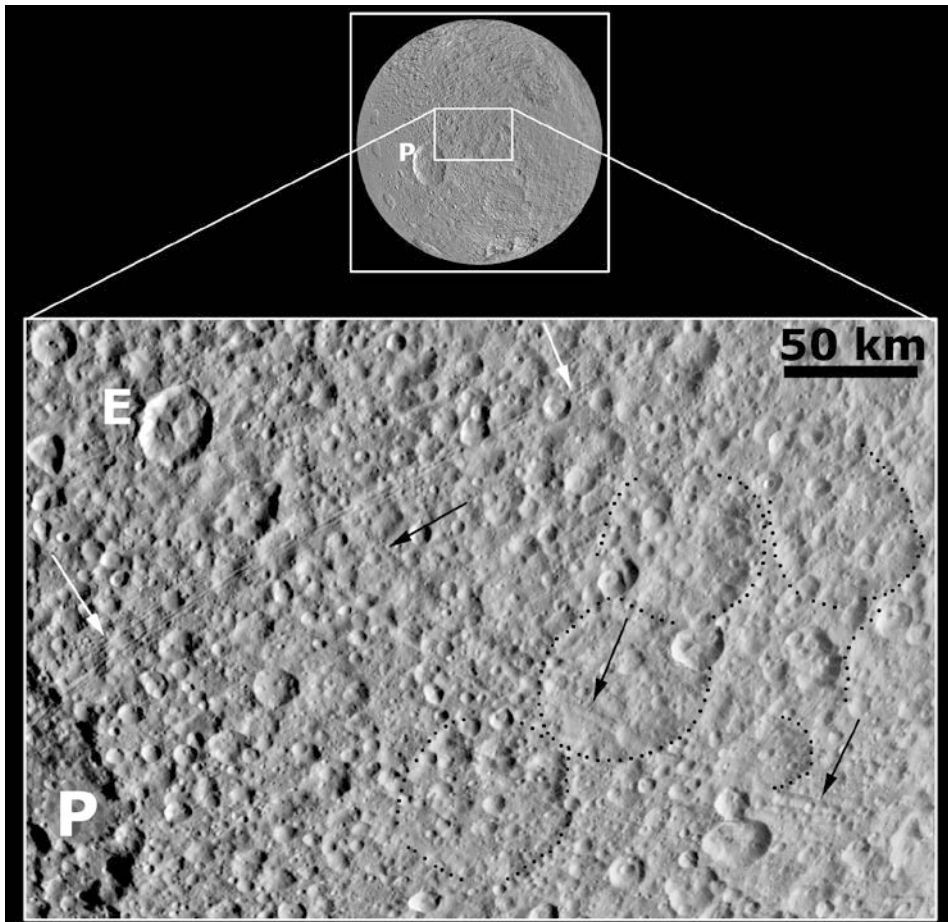
3 Figure 1

4



1

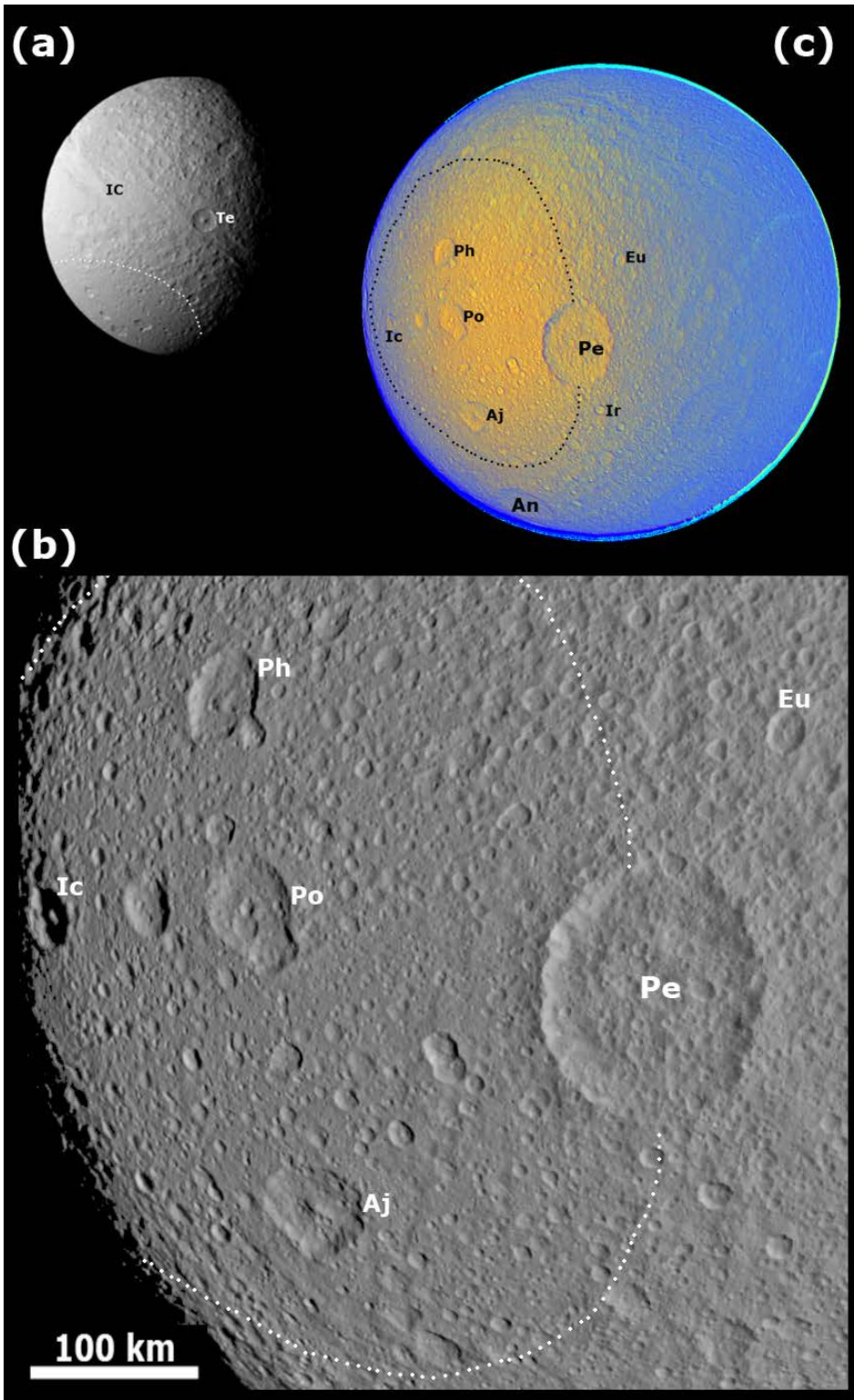
2 Figure 2



1

2

Figure 3

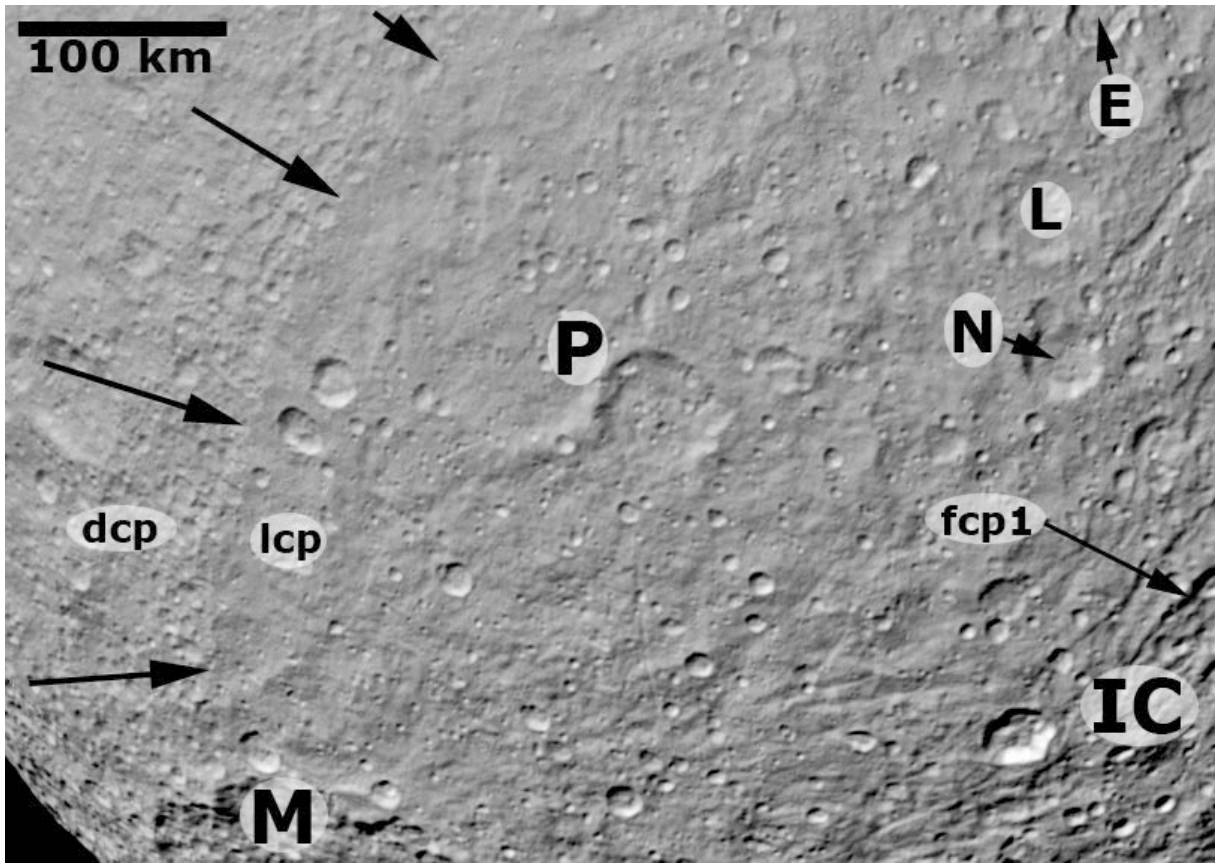


1

2

3

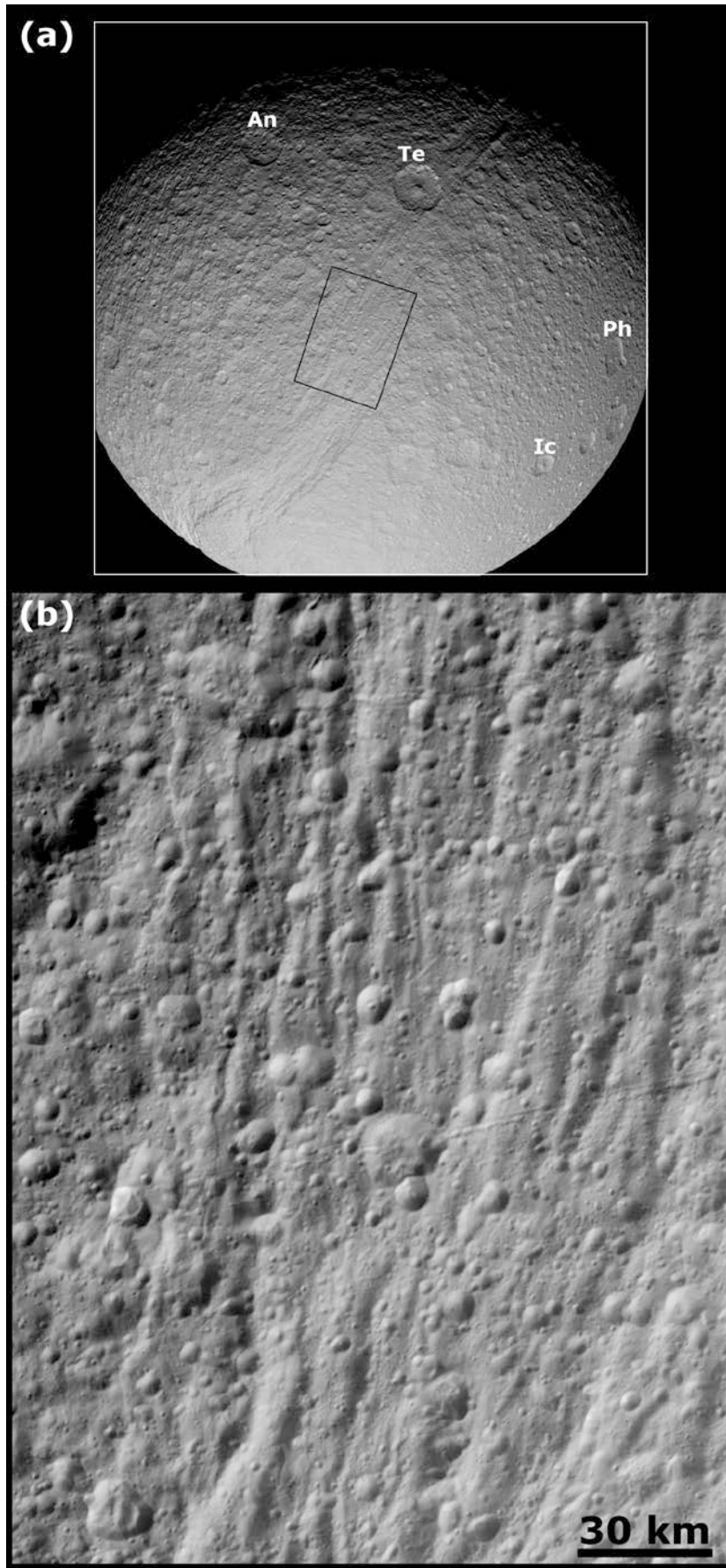
Figure 4



1

2

Figure 5



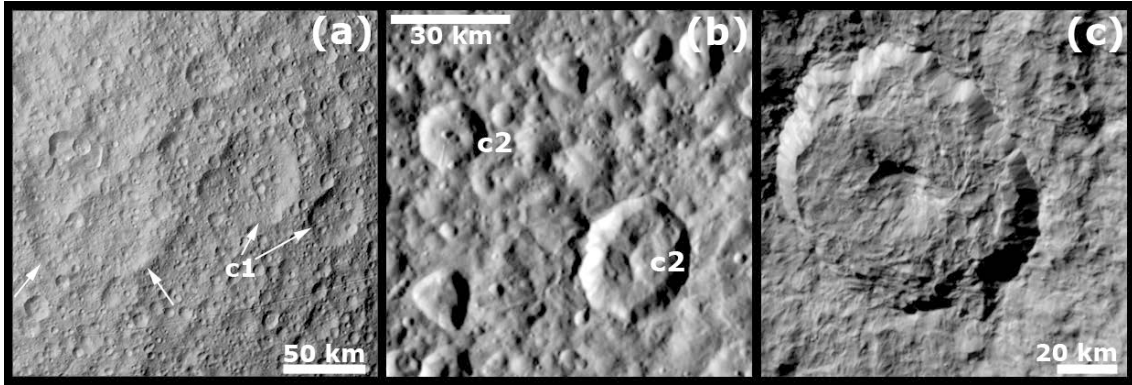
1

2

Figure 6

1

2

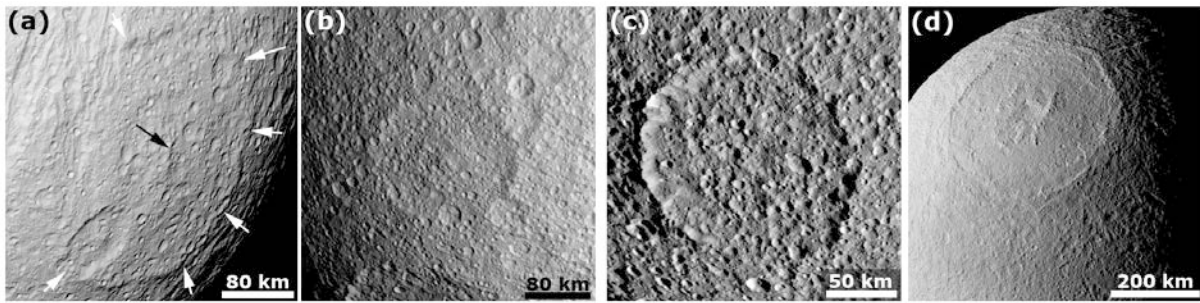


3

4

Figure 7

5

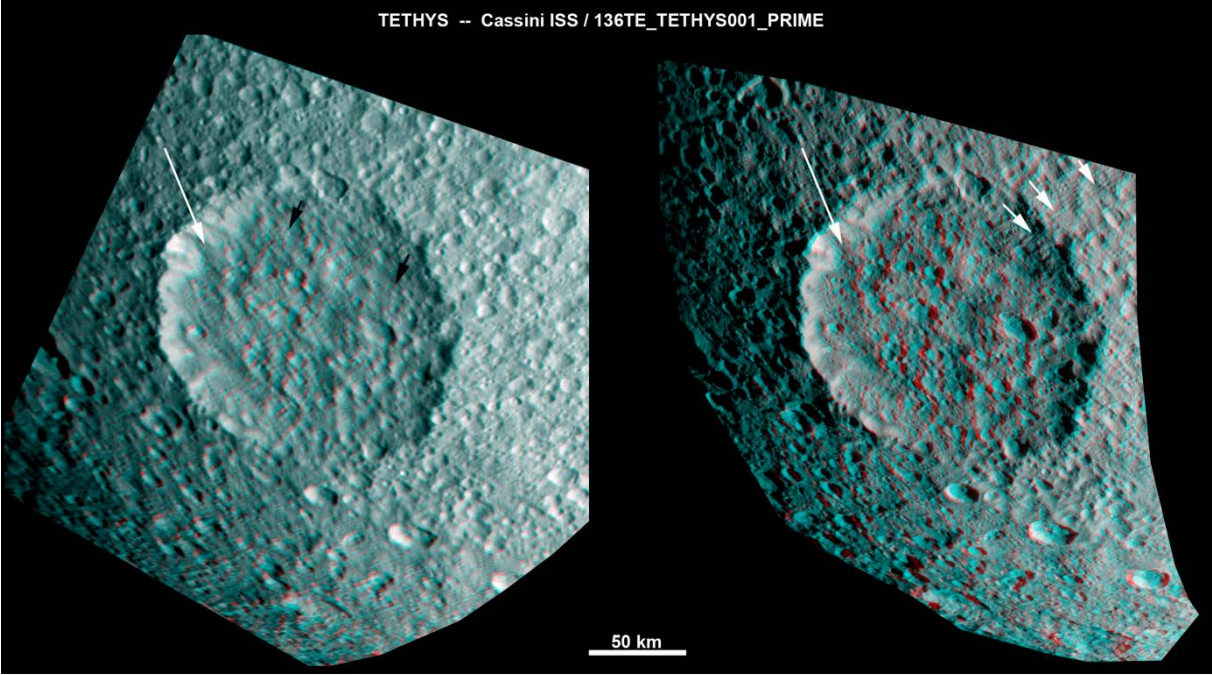


6

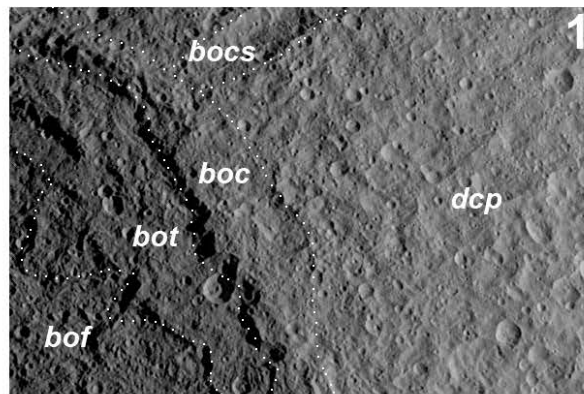
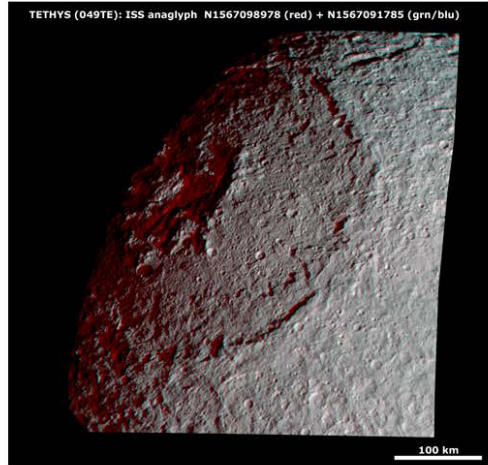
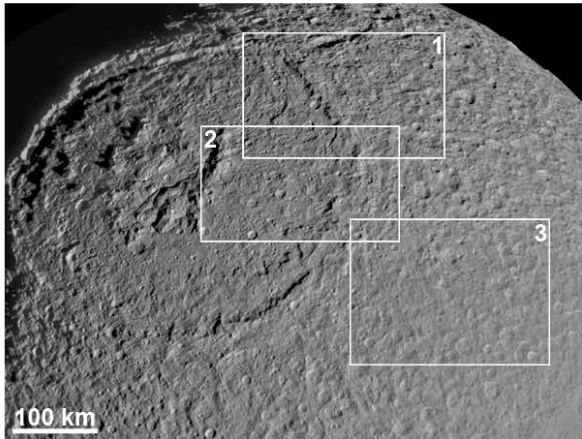
7

Figure 8

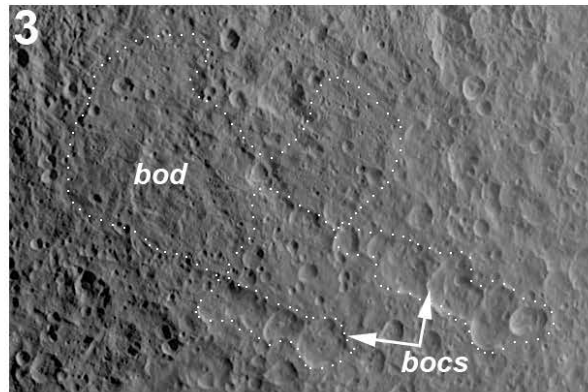
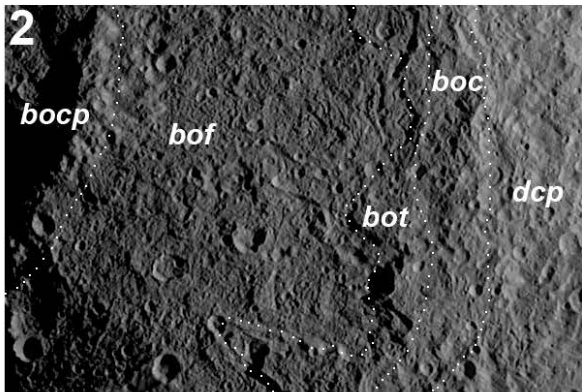
8



2 [Figure 9]



50 km

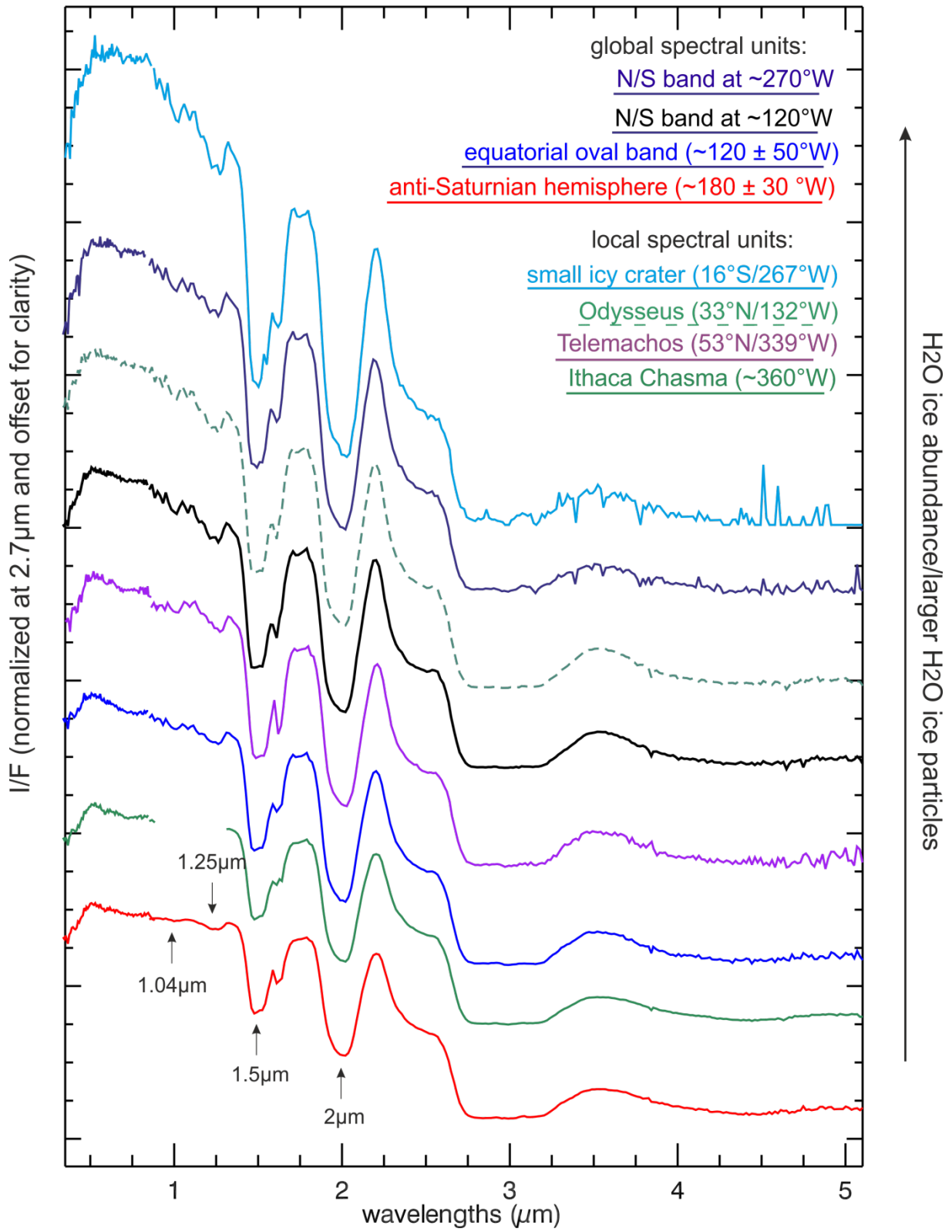


1

2 [Figure 10]

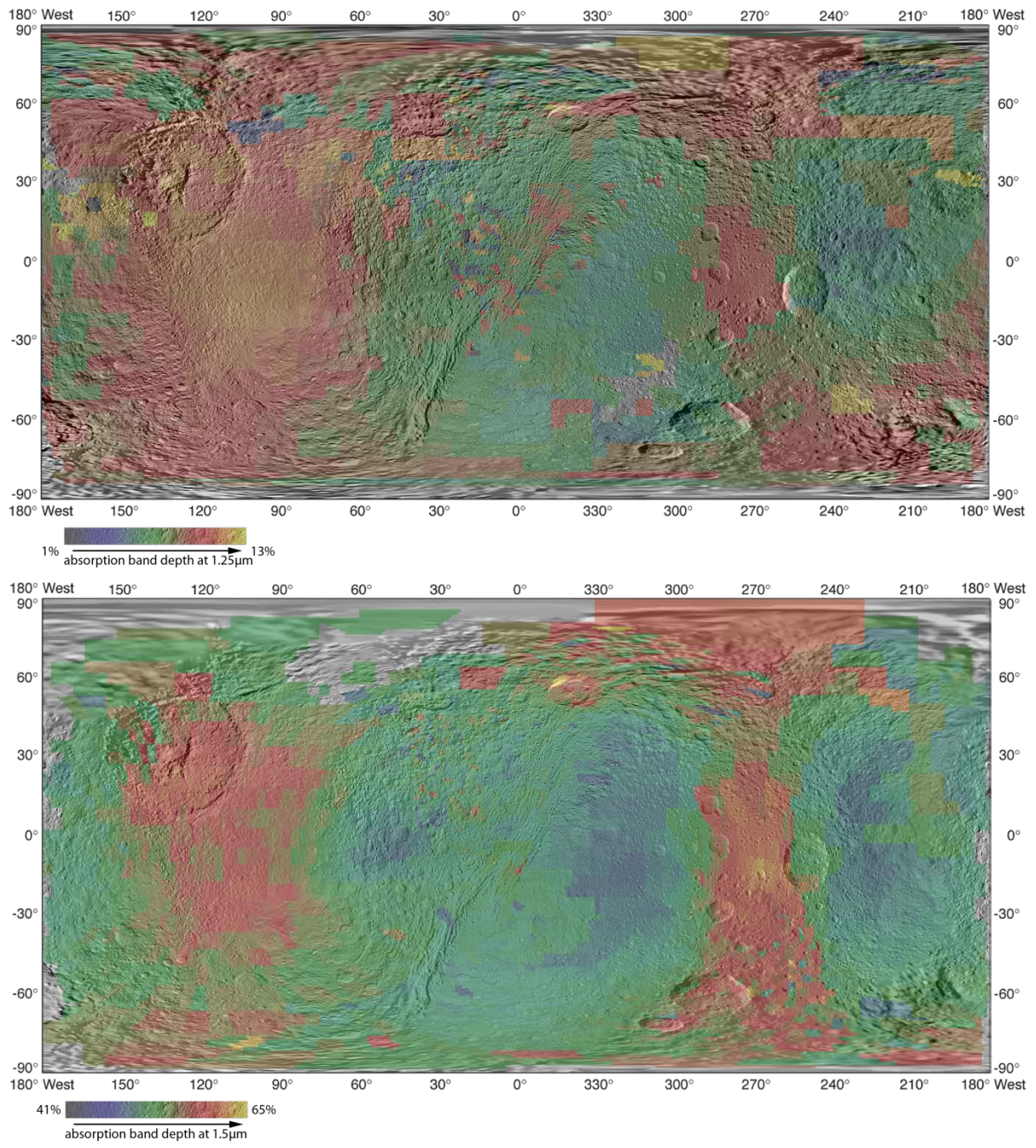
3

4



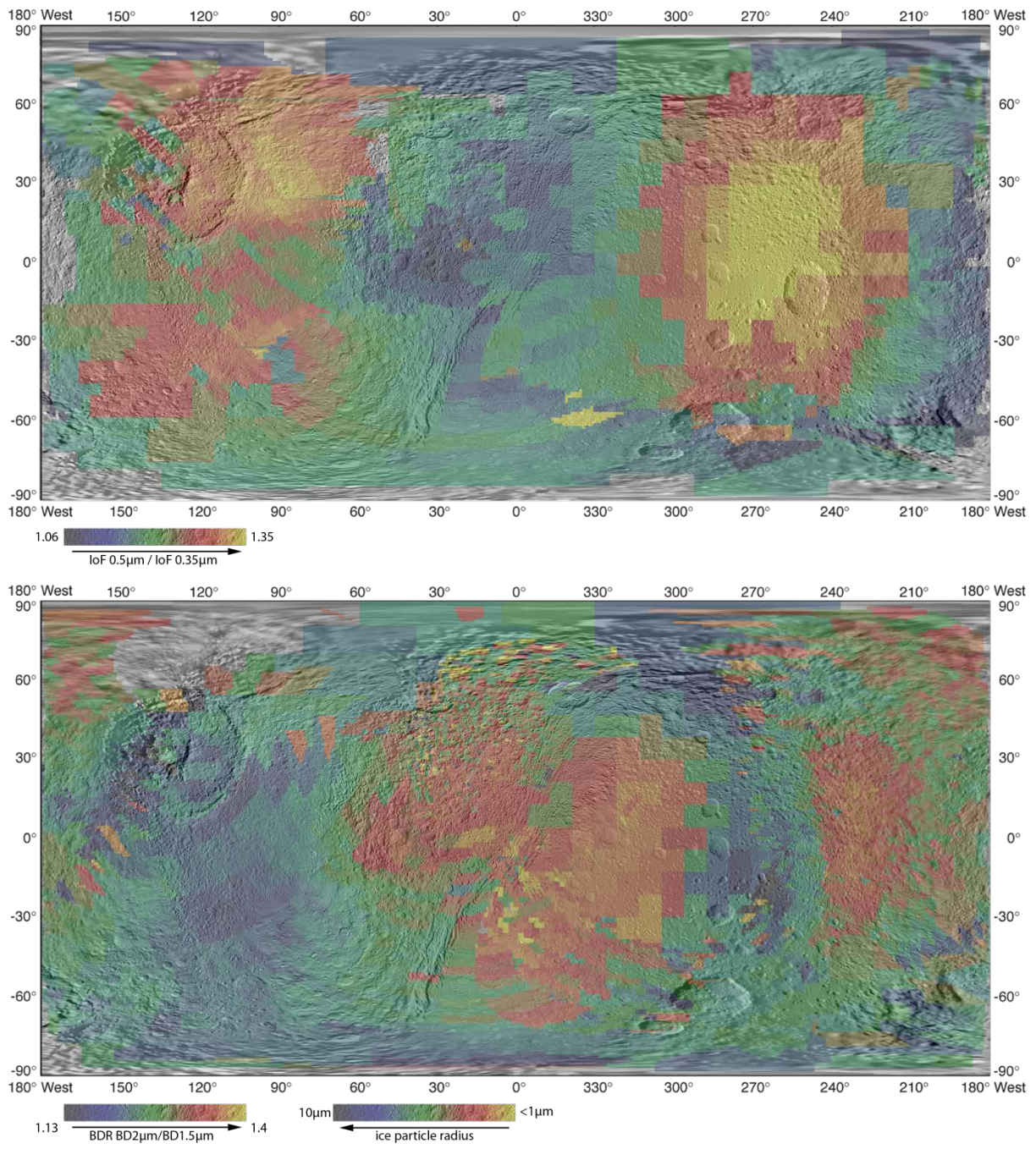
1

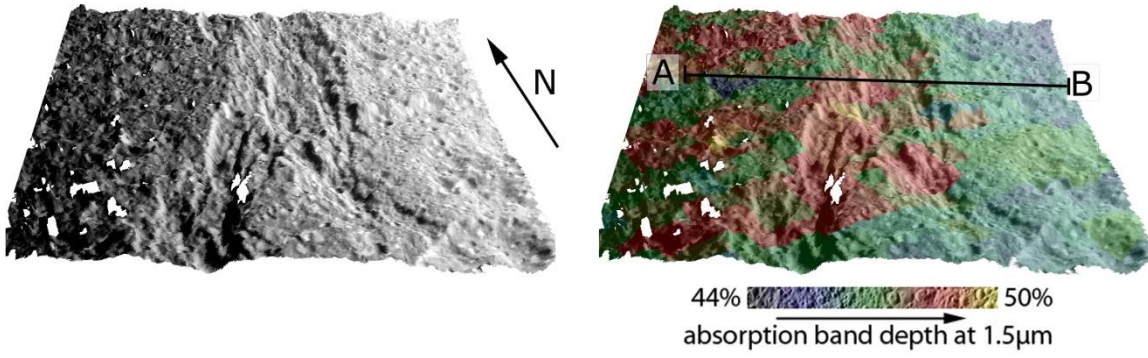
2 [Figure 11]



1

2 [Figure12]

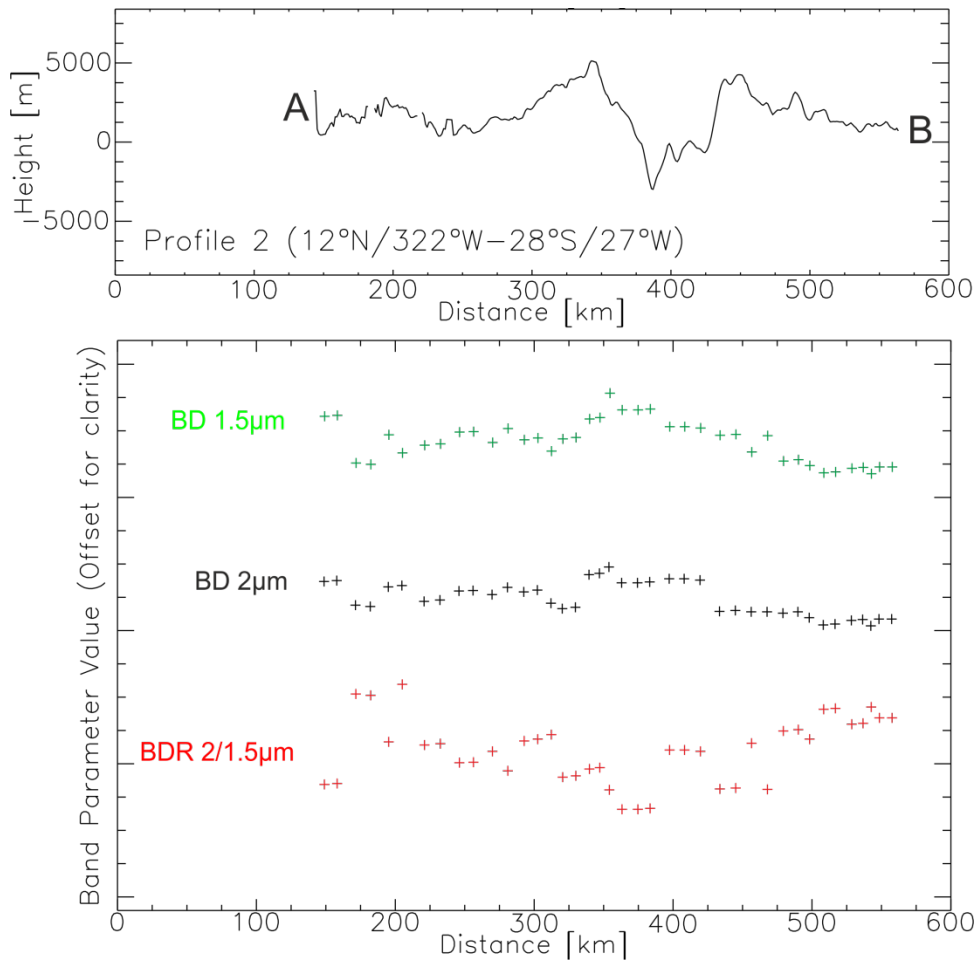




1

2 [Figure 14]

3



4

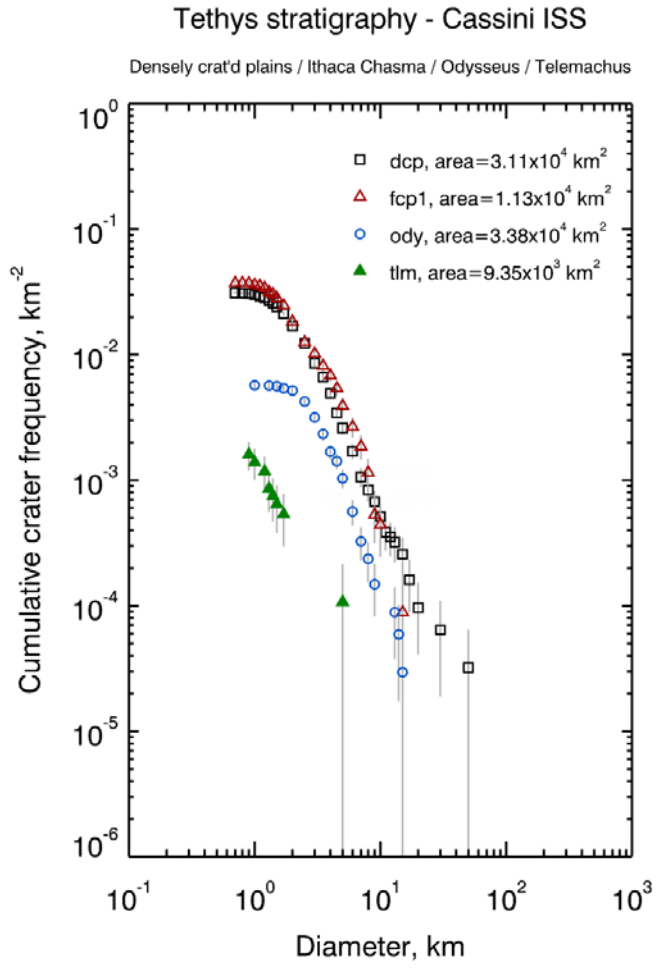
5 [Figure 15]

6

7

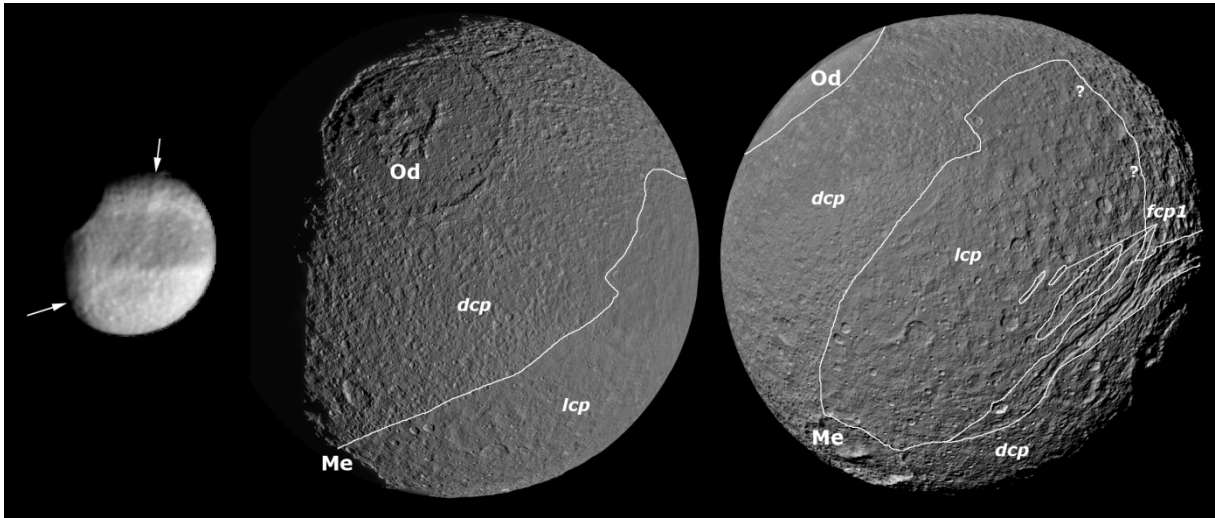
1

2



3

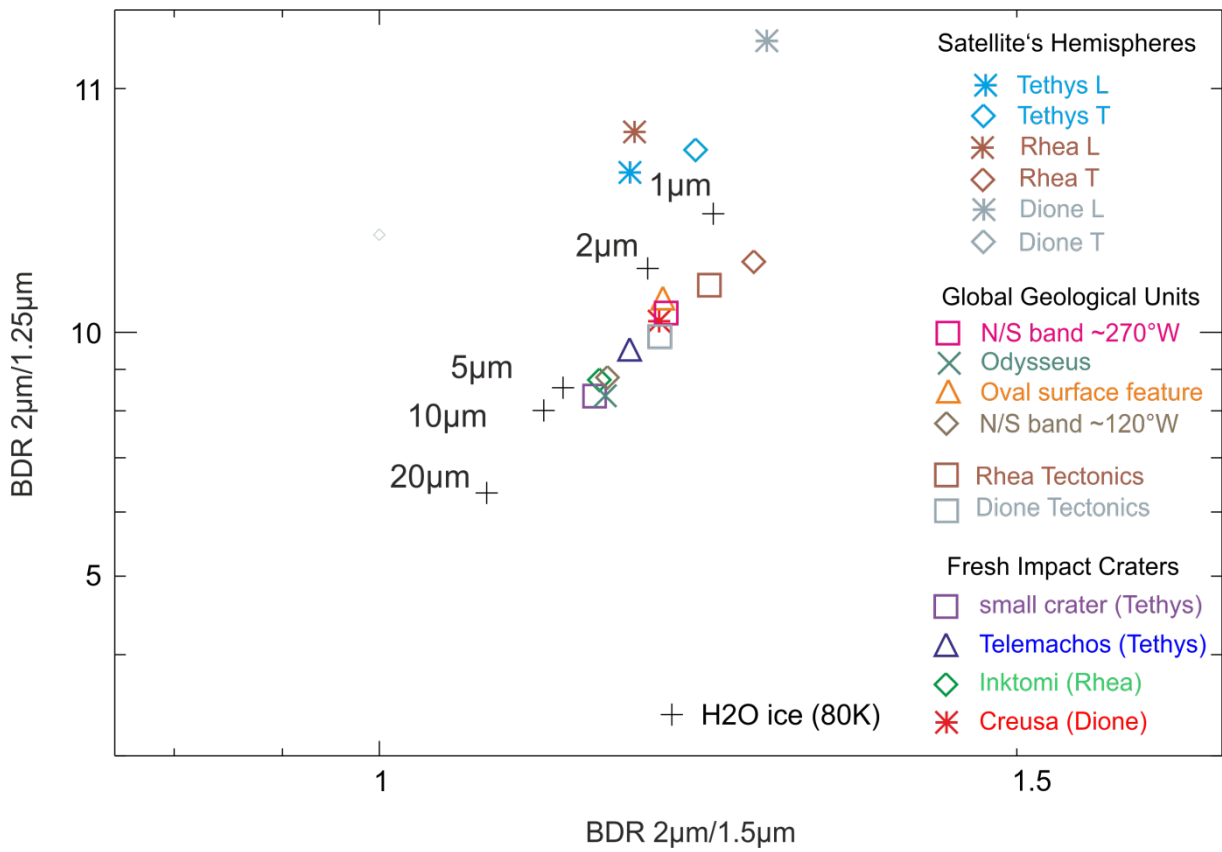
4 [Figure 16]



1

2 [Figure 17]

3



4

5 [Figure 18]

6

1 11 References

- 2 Batson, R. M. (1984), Voyager 1 and 2 atlas of six Saturnian satellites, *NASA Special*
3 *Publication*, 474.
- 4 Brown, R. H., et al. (2004), The Cassini Visual And Infrared Mapping Spectrometer (Vims)
5 Investigation, *Space Sci. Rev.*, 115(1-4), 111-168.
- 6 Buratti, B. J., and J. Veverka (1984), Voyager photometry of Rhea, Dione, Tethys, Enceladus
7 and Mimas, *Icarus*, 58(2), 254-264.
- 8 Buratti, B. J., J. A. Mosher, and T. V. Johnson (1990), Albedo and color maps of the
9 Saturnian satellites, *Icarus*, 87(2), 339-357.
- 10 Buratti, B. J., J. A. Mosher, P. D. Nicholson, C. A. McGhee, and R. G. French (1998), Near-
11 Infrared Photometry of the Saturnian Satellites during Ring Plane Crossing, *Icarus*, 136(2),
12 223-231.
- 13 Chen, E. M. A., and F. Nimmo (2008), Implications from Ithaca Chasma for the thermal and
14 orbital history of Tethys, *Geophysical Research Letters*, 35, 19203.
- 15 Clark, R. N., G. A. Swayze, K. E. Livo, R. F. Kokaly, S. J. Sutley, J. B. Dalton, R. R.
16 McDougal, and C. A. Gent (2003), Imaging spectroscopy: Earth and planetary remote sensing
17 with the USGS Tetracorder and expert systems, *J. Geophys. Res.*, 108(E12), 44.
- 18 Clark, R. N., et al. (2008), Compositional mapping of Saturn's satellite Dione with Cassini
19 VIMS and implications of dark material in the Saturn system, *Icarus*, 193(2), 372-386.
- 20 Clark, R. N., et al. (2012), The surface composition of Iapetus: Mapping results from Cassini
21 VIMS, *Icarus*, 218, 831-860.
- 22 Cruikshank, D. P., et al. (2007), Surface composition of Hyperion, *Nature*, 448(7149), 54-56.
- 23 Dones, L., C. R. Chapman, W. B. McKinnon, H. J. Melosh, M. R. Kirchoff, G. Neukum, and
24 K. J. Zahnle (2009), Icy Satellites of Saturn: Impact Cratering and Age Determination
- 25 Saturn from Cassini-Huygens, edited by M. K. Dougherty, L. W. Esposito and S. M.
26 Krimigis, pp. 613-635, Springer Netherlands.
- 27 Dozier, J. (1989), Remote Sensing of snow in visible and near-infrared wavelengths, in
28 *Theory and Applications of optical remote sensing*, edited by G. Asrar, pp. 527 - 547, John
29 Wiley & Sons.
- 30 Emery, J. P., D. M. Burr, D. P. Cruikshank, R. H. Brown, and J. B. Dalton (2005), Near-
31 infrared (0.8-4.0 μm) spectroscopy of Mimas, Enceladus, Tethys, and Rhea, *Astronomy and*
32 *Astrophysics*, 435(1), 353-362.
- 33 Filacchione, G., et al. (2010), Saturn's icy satellites investigated by Cassini-VIMS, *Icarus*,
34 206(2), 507-523.
- 35 Filacchione, G., et al. (2012), Saturn's icy satellites and rings investigated by Cassini-VIMS:
36 III - Radial compositional variability, *Icarus*, 220, 1064-1096.
- 37 Filacchione, G., et al. (2007), Saturn's icy satellites investigated by Cassini-VIMS: I. Full-disk
38 properties: 350-5100 nm reflectance spectra and phase curves, *Icarus*, 186(1), 259-290.
- 39 Giese, B., R. Wagner, G. Neukum, P. Helfenstein, and P. C. Thomas (2007), Tethys:
40 Lithospheric thickness and heat flux from flexurally supported topography at Ithaca Chasma,
41 *Geophysical Research Letters*, 34(21).
- 42 Giese, B., T. Denk, G. Neukum, T. Roatsch, P. Helfenstein, P. C. Thomas, E. P. Turtle, A.
43 McEwen, and C. C. Porco (2008), The topography of Iapetus' leading side, *Icarus*, 193(2),
44 359-371.
- 45 Hansen, G. B. (2009), Calculation of single-scattering albedos: Comparison of Mie results
46 with Hapke approximations, *Icarus*, 203, 672-676.
- 47 Hansen, G. B., and T. B. McCord (2004), Amorphous and crystalline ice on the Galilean
48 satellites: A balance between thermal and radiolytic processes, *Journal of Geophysical*
49 *Research*, 109(E1).

1 Howett, C. J. A., J. R. Spencer, T. Hurford, A. Verbiscer, and M. Segura (2012), PacMan
2 returns: An electron-generated thermal anomaly on Tethys, *Icarus*, 221, 1084-1088.

3 Hurford, T. A., A. R. Sarid, and R. Greenberg (2007), Cycloidal cracks on Europa: Improved
4 modeling and non-synchronous rotation implications, *Icarus*, 186(1), 218-233.

5 Jaumann, R., R. N. Clark, F. Nimmo, A. R. Hendrix, B. J. Buratti, T. Denk, J. M. Moore, P.
6 M. Schenk, S. J. Ostro, and R. Srama (2009), Icy Satellites: Geological Evolution and Surface
7 Processes, in *Saturn from Cassini-Huygens*, edited by M. K. Dougherty, L. W. Esposito and
8 S. M. Krimigis, pp. 637-681, Springer Netherlands.

9 Jaumann, R., et al. (2008), Distribution of icy particles across Enceladus' surface as derived
10 from Cassini-VIMS measurements, *Icarus*, 193(2), 407-419.

11 Jaumann, R., et al. (2006), High-resolution CASSINI-VIMS mosaics of Titan and the icy
12 Saturnian satellites, *Planetary and Space Science*, 54(12), 1146-1155.

13 Kirchoff, M. R., and P. Schenk (2010), Impact cratering records of the mid-sized, icy
14 saturnian satellites, *Icarus*, 206(2), 485-497.

15 Lucchitta, B. K. (1984), The Galilean Satellite Geological Mapping Program, 1983Rep., 313
16 pp.

17 Moore, J. M., and J. L. Ahern (1983), The geology of Tethys, *J. Geophys. Res.*, 88(S2), A577-
18 A584.

19 Moore, J. M., and P. Schenk (2007), Topography of endogenic features on Saturnian mid-
20 sized satellites, *Lunar Planet. Sci. Conf. XXXVIII*, 1338.

21 Moore, J. M., P. M. Schenk, L. S. Bruesch, E. Asphaug, and W. B. McKinnon (2004), Large
22 impact features on middle-sized icy satellites, *Icarus*, 171(2), 421-443.

23 Moore, J. M., and Ahern, J. L. (1983), The geology of Tethys, *J. Geophys. Res.*, 88, A577-
24 A584.

25 Multhaup, K., and T. Spohn (2007), Stagnant lid convection in the mid-sized icy satellites of
26 Saturn, *Icarus*, 186, 420-435.

27 Neukum, G., R. Wagner, T. Denk, and C. C. Porco (2006), Cratering Chronologies and Ages
28 of the Major Saturnian Satellites, *Geophysical Research Abstracts*, 8(09252).

29 Plescia, J. B., and J. M. Boyce (1982), Crater densities and geological histories of Rhea,
30 Dione, Mimas and Tethys, *Nature*, 295(5847), 285-290.

31 Plescia, J. B., and J. M. Boyce (1985), Impact Cratering History of the Saturnian Satellites, *J.*
32 *Geophys. Res.*, 90(B2), 2029-2037.

33 Porco, C. C., et al. (2004), Cassini Imaging Science: Instrument Characteristics And
34 Anticipated Scientific Investigations At Saturn, *Space Science Reviews*, 115(1), 363-497-497.

35 Roatsch, T., et al. (2009), High-resolution Atlases of Mimas, Tethys, and Iapetus derived
36 from Cassini-ISS images, *Planetary and Space Science*, 57, 83-92.

37 Schenk, P., and J. Moore (2009), Eruptive Volcanism on Saturn's Icy Moon Dione, in *Lunar*
38 *and Planetary Science Conference*, edited, p. 2465.

39 Schenk, P., D. P. Hamilton, R. E. Johnson, W. B. McKinnon, C. Paranicas, J. Schmidt, and
40 M. R. Showalter (2011), Plasma, plumes and rings: Saturn system dynamics as recorded in
41 global color patterns on its midsize icy satellites, *Icarus*, 211(1), 740-757.

42 Schmedemann, N., T. Kneissl, A. Neesemann, G. Michael, R. J. Wagner, C. A. Raymond, and
43 C. T. Russell (2014), The Signature of Secondary Cratering on 4 Vesta and Tethys, in *Lunar*
44 *and Planetary Science Conference*, edited, p. 1960.

45 Smith, B. A., et al. (1981), Encounter with Saturn: Voyager 1 Imaging Science Results,
46 *Science*, 212(4491), 163-191.

47 Smith, B. A., et al. (1982), A New Look at the Saturn System: The Voyager 2 Images,
48 *Science*, 215(4532), 504-537.

49 Spudis, P. D. (1993), *The Geology of Multi-ring Impact Basins*.

1 Stephan, K. (2006), Chemisch-physikalische Zusammensetzung der Ganymedoberfläche:
2 Zusammenhänge mit geologischen Strukturen und deren Gestaltungsprozessen, PhD.
3 Dissertation (in german) thesis.
4 Stephan, K., R. Jaumann, R. Wagner, and J. Castillo-Rogez (2013), Geology of Icy Bodies, in
5 *The Science of Solar System Ices*, edited by M. S. Gudipati, p. 279.
6 Stephan, K., C. A. Hibbitts, R. Wagner, R. Jaumann, and G. B. Hansen (2009), Ganymede's
7 spectral properties: implications for further investigations in a future mission to Jupiter and its
8 satellites, *European Planetary Science Congress*, 4
9 EPSC2009-2633.
10 Stephan, K., et al. (2014), Small fresh impact craters on asteroid 4 Vesta: A compositional
11 and geological fingerprint, *Journal of Geophysical Research (Planets)*, 119, 771-797.
12 Stephan, K., et al. (2010), Dione's spectral and geological properties, *Icarus*, 206(2), 631-652.
13 Stephan, K., et al. (2012), The Saturnian satellite Rhea as seen by Cassini VIMS, *Planetary
14 and Space Science*, 61(1), 142-160.
15 Stooke, P. J. (1989), Tethys: Volcanic and Structural Geology, *Abstracts of the Lunar and
16 Planetary Science Conference*, 20, 1071.
17 Stooke, P. J. (2002), Tethys and Dione: New Geological Interpretations, in *Lunar Planet. Sci.
18 Conf. XXXIII*, edited, Houston, Texas.
19 Teolis, B. D., et al. (2010), Cassini finds an oxygen-carbon dioxide atmosphere at Saturn's icy
20 moon Rhea, *Science*, 330(6012), 1813-1815.
21 Thomas, P. C. (2010), Sizes, shapes, and derived properties of the saturnian satellites after the
22 Cassini nominal mission, *Icarus*, 208, 395-401.
23 Verbiscer, A., R. French, M. Showalter, and P. Helfenstein (2007), Enceladus: Cosmic
24 Graffiti Artist Caught in the Act, *Science*, 315(5813), 815.
25 Wagner, R., K. Stephan, N. Schmedemann, T. Roatsch, E. Kersten, G. Neukum, and C. C.
26 Porco (2013a), Geologic Evolution of Saturn's Icy Moon Tethys, in *AAS/Division for
27 Planetary Sciences Meeting Abstracts*, edited.
28 Wagner, R., K. Stephan, N. Schmedemann, T. Roatsch, E. Kersten, G. Neukum, and C. C.
29 Porco (2013b), Regional geology and stratigraphy of Saturn's icy moon Tethys, in *EGU
30 General Assembly Conference Abstracts*, edited, p. 11009.
31 Wagner, R. J., G. Neukum, N. Schmedemann, T. Roatsch, T. Denk, and C. C. Porco (2012),
32 Clusters of craters on the Saturnian satellite Dione: morphology and size distribution, in
33 *European Planetary Science Congress 2012*, edited, p. 888.
34 Wilhelms, D. E. (1990), Geologic Mapping, in *Planetary Mapping*, edited by R. Greeley, p.
35 208.
36 Zahnle, K., P. Schenk, H. Levison, and L. Dones (2003), Cratering rates in the outer solar
37 system, *Icarus*, 163, 263-289.
38 Zhang, K., and F. Nimmo (2012), Late-stage impacts and the orbital and thermal evolution of
39 Tethys, *Icarus*, 218(1), 348-355.

40

41